Downscaled CMIP6 future climate projections for New Zealand: climatology and extremes

Weather and Climate Extremes 49 (2025) 100784

Contents lists available at ScienceDirect

Weather and Climate Extremes

journal homepage: www.elsevier.com/locate/wace

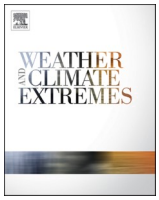

Downscaled CMIP6 future climate projections for New Zealand: climatology and extremes

Peter B. Gibson [a,*], Ashley M. Broadbent [a], Stephen J. Stuart [a], Hamish Lewis [a,b], Isaac Campbell [a], Neelesh Rampal [a], Luke J. Harrington [b], Jonny Williams [c]

[a] National Institute of Water and Atmospheric Research (NIWA), New Zealand
[b] Te Aka Mātuatua School of Science, University of Waikato, Hamilton, 3216, New Zealand
[c] Department of Meteorology, University of Reading, Reading, United Kingdom

ARTICLE INFO

Keywords:
Regional modelling
Regional climate
Precipitation extremes
Drought
Heatwaves

ABSTRACT

Downscaled climate projections provide regionally relevant information for climate adaptation and planning purposes. Updated climate projections (~12-km) are presented here for the New Zealand region, downscaling 6 global climate models (GCMs) from the Coupled Model Intercomparison Project (CMIP6) under a high emissions scenario (SSP3-7.0). Three regional climate models (RCMs) are used to explore differences when downscaling select GCMs. For end of century projections (relative to 1986–2005), the national multi-model annual mean warming is 3.1°C (model range 2.0–3.8°C) across downscaled simulations. Downscaling generally enhances warming over New Zealand relative to the GCMs, with the largest increases across high-elevation regions. There can be important differences in the projections across RCMs, including at national scales for temperature and across local-to-regional scales for precipitation. Averaged across models, annual extreme heatwaves become 3–5°C hotter for most regions. More frequent, intense, and longer duration meteorological drought is projected across northern and eastern regions of both islands. In terms of model uncertainty based on sign agreement, while summer mean precipitation projections carry the largest uncertainty, projections of summer meteorological drought and precipitation extremes can be made with greater confidence. These results provide a foundation for further targeted regional climate change impact and adaptation studies.

1. Introduction

The provision of robust quantitative projections of climate extremes on regional scales remains a grand challenge for climate science (Marotzke et al., 2017; Palmer and Stevens, 2019; Jakob et al., 2023). Alongside the scientific challenge, since planning for climate adaptation typically occurs across local and regional scales, there is growing demand from stakeholders for higher-resolution information about changing climate risk (Giorgi, 2019; Fiedler et al., 2021; Gonçalves et al., 2022).

Especially in complex terrain and island settings, the output from global climate models (GCMs) generally has limited direct utility across local through regional scales (Giorgi, 2019; Gibson et al., 2024a; Evans et al., 2024). Across much of Aotearoa New Zealand, orographic precipitation, mountain-valley winds, and land-sea breezes are highly important features of the mesoscale circulation yet are generally poorly represented in coarse resolution GCMs (Stone et al., 2022; Gibson et al., 2024a). Other important features of the synoptic scale atmospheric circulation are also challenging to represent in GCMs, which are often better captured in downscaling from high-resolution regional climate models (RCMs). These include tropical and ex-tropical cyclones (Gibson et al., 2024a) and atmospheric rivers and associated precipitation (Rhoades et al., 2020; Payne et al., 2020), which are key drivers of extreme precipitation across New Zealand (e.g. Lorrey et al., 2014; Prince et al., 2021; Shu et al., 2021; Harrington et al., 2023). This highlights the important role of dynamical downscaling for refining climate projections of extreme events, especially for island nations and regions of complex terrain like New Zealand.

Earlier regional climate model simulations for New Zealand have been produced through dynamical downscaling of reanalysis and Coupled Model Intercomparison Project Phase 3 (CMIP3, and earlier) (MfE et al., 2008). Most of these early regional modelling studies for New Zealand focused on model setup and evaluation (e.g. Renwick et al., 1998; Drost et al., 2007; Ackerley et al., 2012), with less direct

* Corresponding author.
E-mail address: peter.gibson@niwa.co.nz (P.B. Gibson).

https://doi.org/10.1016/j.wace.2025.100784
Received 18 September 2024; Received in revised form 7 March 2025; Accepted 28 May 2025
Available online 29 May 2025

focus on future climate projections.

For CMIP5, future downscaled projections with HadAM3P/HadRM3P (~30-km resolution over New Zealand) were documented in MfE (2018), which are summarized here. Future warming is projected to be largest in summer, with the highest rates of warming in high-elevation regions. Daily maximum temperatures warm faster than minimum temperatures overall, increasing the diurnal temperature range. For mean precipitation, the largest and most consistent projections were for winter, with increases of up to 40 % in parts the South Island West Coast under the high-emissions scenario of RCP8.5 by end-of-century. Moderate intensity precipitation extremes are projected to increase over most of the country. Drought intensity, as defined by potential evapotranspiration deficit, is projected to increase in most places, with the largest increases often occurring in already dry water-stressed regions such as the north and east of the North Island, and the lee of the Southern Alps in the South Island. Various downstream climate change applications have also been studied through these CMIP5 downscaled projections, including for hydrological projections (Jobst et al., 2018; Akhter et al., 2019; Collins, 2020), fire weather (Melia et al., 2022), and rainfall-induced damages from flooding and landslips (Pastor-Paz et al., 2020).

More recently, for CMIP6 projections, Gibson et al. (2024b) documented the spread in precipitation projections for New Zealand across the full GCM ensemble (prior to downscaling) through a 'storylines' framework. A regional process-based context for projections of mean precipitation was provided, highlighting the important role of how projected changes in associated large-scale circulation features (e.g. the jet, Hadley cell, Rossby waves) differ between summer and winter. It was also pointed out that summer precipitation projections can be strongly dominated by internal variability alone in certain GCMs, providing important context for interpreting uncertainty in regional projections.

For CMIP6 downscaling, a recent accompanying study (Gibson et al., 2024a) has described the experiment design, with the Conformal Cubic Atmospheric Model (CCAM, Thatcher and McGregor, 2009) used as the primary model for downscaling. That study comprehensively evaluated the downscaled output over the historical period, from the perspective of added value versus the driving GCMs. Some of the main areas of added value include wide-spread and improvements to the maximum and minimum temperature climatology, and large improvements to orographic precipitation. Interannual variability in temperature was also shown to be in close agreement with observations. For extreme events, large and consistent improvements were also found for several temperature and precipitation-based extreme indices. Large improvements to the representation of tropical cyclone statistics are also apparent in the downscaled output, especially across the category 2 and 3 intensity range, though very intense tropical cyclones (category 4+) are still underrepresented in CCAM and to a similar degree in ERA5 reanalysis (Gibson et al., 2023). CCAM has also been comprehensively evaluated for this region from the perspective of large-scale atmospheric circulation conditions, when driven from prescribed/observed sea surface temperature (SST) and sea ice concentration (SIC) (Gibson et al., 2023).

Building upon these historical evaluation studies (Gibson et al., 2023, 2024a), the overarching goal of this study is to provide a wide-ranging summary of updated (i.e. CMIP6) national climate projections for New Zealand, including for extreme events. We explore the following research questions: How do the RCMs modify the climate projections relative to the GCMs? How do the projections differ across RCMs for downscaling a given GCM? How are extreme events, such as heatwaves and drought, projected to change? How does uncertainty in the projections compare across variables, extreme indices, and seasons? Many of these research questions, such as RCM intercomparisons and uncertainty quantification, have not been investigated before for this region. We anticipate that by covering a wider range of research questions, this will provide the necessary foundations for future research on extremes with more in-depth process-based examinations of the drivers. The remainder of the paper is structured as follows. Section 2 (Methods) provides an overview of the downscaling experiment design and various indices for extreme events. Section 3 (Results and Discussion) presents the updated climate projections and discusses these in the context of earlier CMIP3/5 projections. Lastly, the main findings are summarized in Section 4 (Conclusions).

2. Methods

2.1. CMIP6 downscaling experiment design

The experiment design has been comprehensively described in a recent separate paper (Gibson et al., 2024a). Here, we briefly summarize the most relevant and important points. The primary dynamical model used for downscaling was CCAM (Thatcher and McGregor, 2009), specifically version CCAM-2206. A global stretched grid configuration (C288) was implemented in CCAM focusing high-resolution over New Zealand (~12-km) accompanied by relatively high resolution (~12-35-km) over a much wider region spanning the South Pacific. As discussed in Gibson et al. (2023), this stretched grid configuration has additional attractive properties, including for the representation of storms as they approach the domain of interest. Additionally, the stretched grid removes certain issues concerning the size and placement of domain boundaries from traditional limited area RCMs. Further technical details on the CCAM configuration, including the grid and physics schemes, are provided in Gibson et al., (2024a).

As described in Gibson et al. (2024a), the GCM selection for downscaling was based on carefully balancing several factors: model performance in the region over the historical period (including for features of the large-scale circulation and teleconnections), model independence, rate of future warming, and data availability. Details of the six CMIP6 GCMs selected for downscaling are shown in Table 1. As shown in Gibson et al. (2024a), the six selected GCMs span the overall CMIP6 ensemble warming range well (in both a global and New Zealand context), while additionally being constrained to the Intergovernmental Panel on Climate Change (IPCC) 'very likely range' for Equilibrium Climate Sensitivity (ECS) to avoid the oversampling of 'hot models'

Table 1
Details for the downscaling experiment design. Each RCM has an atmospheric grid resolution of approximately 12 km over the New Zealand region. Further details of the model setup are given in Section 2. For ACCESS-CM2, r4i1p1f1 was used due to data availability. GCM atmospheric resolution is approximate. RCM simulations marked with asterisks are primarily used for exploring RCM uncertainty and were not included when computing multi-model mean statistics.

Host GCM (variant label) Atmospheric resolution	RCM (12 km)	Model setup for downscaling
ACCESS-CM2 (r4i1p1f1) 1.875° x 1.25°	CCAM	Global spectral nudging to atmospheric and SST/SIC fields from GCM
	WRF*	Lateral boundary conditions from atmospheric and SST fields from GCM
NZESM (r1i1p1f1) 1.875° x 1.25°	CCAM*	Global spectral nudging to atmospheric and SST/SIC fields from GCM
	UM*	Lateral boundary conditions from atmospheric and SST fields from GCM
NorESM2-MM (r1i1p1f1) 1.0° x 1.0°	CCAM	Global spectral nudging to atmospheric and SST/SIC fields from GCM
EC-Earth 3 (r1i1p1f1) 0.7° x 0.7	CCAM	Global spectral nudging to atmospheric and SST/SIC fields from GCM
GFDL-ESM4 (r1i1p1f1) 1.0° x 1.0°	CCAM	Global atmospheric CCAM simulation (no atmospheric nudging) with SST/SIC fields from GCM
AWI-CM-1-1-MR (r1i1p1f1) 0.94° x 0.94°	CCAM	Global atmospheric CCAM simulation (no atmospheric nudging) with SST/SIC fields from GCM
CNRM-CM6-1 (r1i1p1f2) 1.4° x 1.4°	CCAM	Global atmospheric CCAM simulation (no atmospheric nudging) with SST/SIC fields from GCM

(Hausfather et al., 2022). Other aspects of the ensemble, such as the sampling of rainfall and circulation projections are discussed in Gibson et al. (2024a,b).

Additionally, there is flexibility in how the input data from the GCMs is used to drive CCAM. One option is to apply spectral nudging to a range of atmospheric fields (i.e. temperature, pressure, and wind fields at multiple vertical levels) from the host GCM (e.g. Thatcher and McGregor, 2009). Another option is to run CCAM in 'AMIP'-mode, driven only by global SST/SIC fields from the host GCM (e.g. Hoffmann et al., 2016; Chapman et al., 2023). The latter option further enables an opportunity to bias-correct SST fields from the host GCM before being ingested into CCAM which can lead to improvements in the representation of downscaled precipitation and other fields (Hoffmann et al., 2016; Chapman et al., 2023). Both approaches carry their own advantages and disadvantages (see Gibson et al., 2024a for further details), and have been combined and considered part of an ensemble of regional climate projections (Grose et al., 2023). As detailed in Table 1, three GCMs have been downscaled through direct spectral nudging and another three GCMs downscaled through bias-corrected SST/SIC-driven simulations. Each of these GCMs was downscaled with time varying CMIP6 forcings (i.e. greenhouse gas, aerosol, ozone, and solar) over the historical period (years 1960–2014) and for various future scenarios (SSP1-2.6, SSP2-4.5, SSP3-7.0, years 2015–2099).

For the analysis presented here, we focus on the SSP3-7.0 scenario as it represents a high-emissions scenario from which the climate change response can more readily be separated from internal variability, while alleviating some of the concerns expressed around the realism and suitability of the stronger forcing scenario represented by SSP5-8.5 (e.g. Hausfather and Peters, 2020). The results presented here for SSP3-7.0 should not be interpreted as the 'most likely' scenario but instead as a feasible and approximate upper limit for change. While the focus here is not directly on scenario uncertainty, comparisons of the climate projections across other SSPs (in terms of the spatial pattern of the change) were assessed for select variables.

While CCAM was the primary dynamical model for downscaling, two other limited area RCMs were also run in a more limited setting (see Campbell et al., 2024a for details). These were: the Advanced Research version of the Weather Research and Forecasting (WRF) (version 4.3) RCM (Skamarock and Klemp, 2008) and the Unified Model (UM) RCM based on the Global Atmosphere 7 (GA7, Walters et al., 2019) configuration of the UK Met Office Unified Model. To address important research questions, future climate projections from these two other RCMs were compared against CCAM by downscaling a common GCM (see Table 1). For example, how do the climate projections compare when WRF is used instead of CCAM for downscaling ACCESS-CM2? While not officially part of CMIP6, New Zealand Earth System Model (NZESM) GCM (Williams et al., 2016; Behrens et al., 2020) was also downscaled by both CCAM and the UM (Table 1) with the downscaled output is compared here. We note that the atmospheric component in NZESM is very similar to ACCESS-CM2 (Bi et al., 2020), both based on UM GA7.1, but with different ocean models and resolutions.

2.2. ETCCDI indices

Climate projections were assessed for select temperature and precipitation-based indices (Table 2) from the Expert Team on Climate Change Detection and Indices (ETCCDI, Zhang et al., 2011). This enabled different parts of the statistical distribution to be considered as well as duration-based aspects (e.g. the length of wet and dry spells). For these indices, and other fields/indices, climate projections were computed as the time-averaged difference between years 2080–2099 and years 1986–2005, under SSP370. The base period of 1986–2005 was used here to facilitate comparisons against earlier CMIP5 projections MfE (2018). We also assess the ratio of the change in TXx (hottest annual day) and 'tas' (annual-mean daily mean temperature). This ratio is used to assess whether the warm tail of the daily temperature distribution is warming faster than the mean, across different regions and models. This ratio (i.e. TXx/tas) has been commonly applied in other regions and studies, often in the context of studying land-atmosphere feedbacks (e.g. Seneviratne et al., 2016; Donat et al., 2017, 2018; Vogel et al., 2017).

Table 2
Extreme event ETCCDI indices evaluated across models in this study.

Index name	Description	Input variable (daily)
CWD	Annual maximum wet spell length (consecutive days pr $\geq$ 1 mm)	pr
R1mm	Annual number of wet days (pr $\geq$ 1 mm)	pr
Rx1day	Annual maximum 1-day precipitation	pr
Rx3day	Annual maximum 3-day precipitation	pr
SDII	Average daily precipitation on wet days (pr $\geq$ 1 mm)	pr
DTR	Daily temperature range	tmin, tmax
FD	Annual number of frost days (daily tmin $< 0^{\circ}$C)	tmin
Tmax	Annual average of daily tasmax	tmax
Tmin	Annual average of daily tasmin	tmin
TXx	Annual maximum of daily tasmax	tmax
TNn	Annual minimum of daily tasmin	tmin

2.3. Heatwave indices

While some aspects of hot extremes are included in Table 2, these do not include duration-based considerations, such as multi-day heatwaves. For this reason, we extend our analysis to include heatwaves following the framework of Perkins and Alexander (2013). Through this approach, heatwaves are calculated based on the daily maximum temperature ('tasmax') exceeding the 95th percentile relative to the time of year (i.e. 15-day moving window) and location (i.e. percentiles computed on a grid cell basis). Additionally, the exceedance of the 95th percentile must occur for at least 3 consecutive days to be counted as part of a heatwave. The percentiles are computed across the historical period (1960–2014). From this, we consider three heatwave metrics, as defined in Perkins and Alexander (2013). These are the heatwave frequency (HWF, i.e. the annual number of heatwave days), the heatwave amplitude (HWA, the temperature on the hottest day of the hottest annual heatwave), the heatwave duration (HWD, the duration of the longest heatwave event annually). We restrict the analysis to an extended southern hemisphere summer period (November through March).

2.4. Drought indices

We analyse meteorological drought (i.e. rainfall deficits) following the method described in Ukkola et al. (2020). This approach defines drought based on the 15th percentile of the 3-month running mean of precipitation, then applied to each month. The percentiles are computed for each location (i.e. grid cell) across the historical period (1960–2014). From this, following Ukkola et al. (2020), a drought event is defined as a month, or a number of consecutive months, when the running mean precipitation is below the drought threshold. Drought frequency is defined as the annual (or seasonal) number of drought events according to the drought threshold. Drought duration is longest consecutive drought event for a given period (i.e. annual or seasonal). Drought intensity is defined as the difference between the drought threshold and the monthly running mean precipitation.

2.5. Uncertainty metric

A relatively simple and informative way to present uncertainty in climate projections is to assess the level of sign agreement across individual models within the ensemble. This is particularly relevant for projections of precipitation, where the multi-model mean may obfuscate changes across models due to sign disagreement, including across the New Zealand region (Gibson et al., 2024b). This is commonly used in

IPCC Assessment reports (e.g. Lee et al., 2021), where hatching on maps is used to indicate model sign agreement above a certain threshold. From this we quantify the percentage of land (i.e. over New Zealand) in which there is sign agreement across models at a particular level (e.g. 4 of 6 models agree, or 5 of 6 models agree). This provides a summary metric where projection uncertainty can be readily compared across multiple climate variables, indices and seasons. Given limitations of the ensemble size here, it is important to caveat that this does not encompass the full extent of uncertainty (Palmer and Räisänen, 2002; Giorgi, 2019), and even when all models in the ensemble agree this should not be interpreted that there is no uncertainty in the projections. This is related to the practical necessity of selecting a subset of models, which inherently limits the range of all possible modelling options, including across both global and regional models (Knutti et al., 2013).

3. Results and Discussion

3.1. Temperature

We begin by showing climate projections, defined as the future period climatology minus historical climatology (years 2080–2099 minus years 1986–2005), for temperature across different GCMs. We also explore how downscaling modifies the climate change pattern response relative to the raw GCM output, and how this differs across RCMs. Spatial maps for projections of daily mean annual temperature ('tas') are shown in Fig. 1. The national average projected warming is 3.1°C (model range 2.0–3.8°C) across downscaled models. Relative the host GCM, downscaling from CCAM enhances the nationally averaged tas warming by up to +0.5°C. Compared to other seasons and temperature statistics, the warming for summer tasmax is overall the largest. For tasmax in summer, warming tends to be enhanced more so across inland regions of the North Island (Supplementary Material Fig. S1), with national average projected warming of 3.9°C (model range 2.8–4.8°C) across downscaled models.

Compared to the GCM, downscaling tends to also show enhanced warming over regions of high elevation of the South Island, which is shown in greater detail in Fig. 2 by separating daily maximum (tasmax) and minimum temperature (tasmin) changes. This elevation-dependent warming is most apparent in winter (JJA), where all RCMs (CCAM, WRF, UM) show evidence for this, though the spatial patterns and magnitudes differ somewhat across RCMs when driven by the same GCM. Enhanced high elevation warming is consistent with previous CMIP5 downscaled projections MfE (2018) and appears primarily related to reduced surface albedo from reduced snow cover and reduced snowfall with warming into the future. This is suggested to be more pronounced in the RCMs than the GCMs due to representation of topography that is lacking at the typical GCM resolution. Given the differences between the tasmax and tasmin changes shown in Fig. 2, and the differences across RCMs, it is likely that more complex changes to clouds, water vapor and radiative fluxes (Pepin et al., 2015; Campbell et al., 2024) are also playing an important role which will be explored in future work.

The nationally averaged projections for tasmax are further analysed in Fig. 3 to examine differences between RCMs. Downscaling CCAM in 'AMIP mode' (driven only by SST/SIC) tends to produce a greater warming rate relative to the GCM. This is evident in Fig. 3 where the red points (CCAM driven with SST/SIC) are typically further from the 1:1 warming slope compared to the grey points (CCAM driven with atmospheric nudging), where the 1:1 warming slope indicates equal warming from the GCM and RCM. The use of multiple RCMs also allows us to compare projections when downscaling select GCMs (i.e. ACCESS-CM2 is downscaled by both CCAM and WRF; the NZESM is downscaled by both CCAM and UM). Overall, for tasmax across different seasons, the changes are very similar across CCAM and UM, where both RCMs slightly enhance warming by +0.1°C relative to NZESM. In contrast, larger differences are apparent when comparing CCAM and WRF. For example, in summer, the warming from CCAM is approximately +0.9°C relative to WRF, when both RCMs are downscaling ACCESS-CM2.

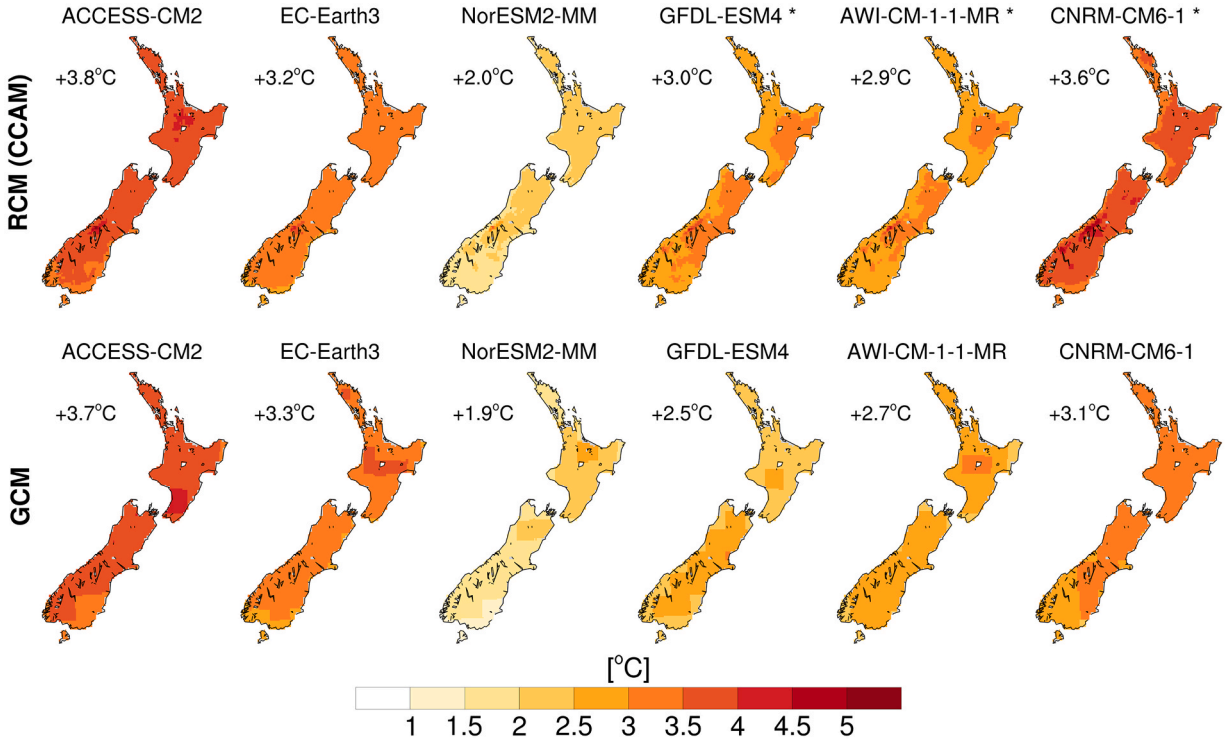

Fig. 1. Climate projections (years 2080–2099 minus years 1986–2005) under SSP370 for annual mean temperature (tas). The values in the top left of each panel are for the NZ-averaged change. The top row shows the RCM (CCAM) and the bottom row shows each GCM (i.e. prior to downscaling). Asterisks indicate that only the SST/SIC fields from the GCM have been used to drive CCAM.

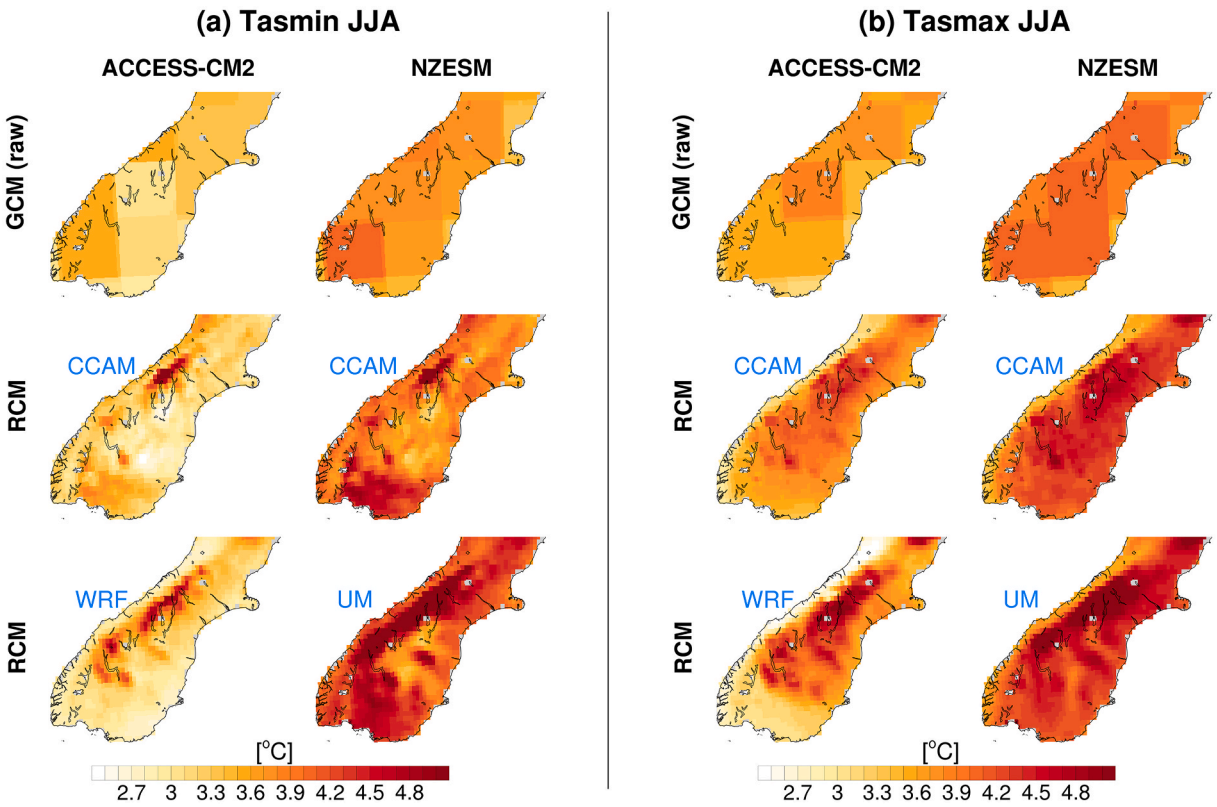

Fig. 2. Climate projections (years 2080–2099 minus years 1986–2005) under SSP370 for daily minimum temperatures (tasmin, panel a) and daily maximum temperatures (tasmax, panel b) in winter (JJA). The ACCESS-CM2 model is downscaled with CCAM and WRF; NZESM is downscaled with CCAM and UM.

Further processed-based evaluations of these two model simulations would be useful for shedding light on what is responsible for this difference, including analysis of cloud cover changes (Campbell et al., 2024) and land-atmosphere feedbacks (e.g. Donat et al., 2017).

Another important consideration is understanding why warming appears to be enhanced more so in CCAM SST/SIC-driven simulations compared to the nudged simulations relative to each host GCM, especially in the summer season. While both approaches are commonly used for downscaling with CCAM (Grose et al., 2023; Chapman et al., 2023), to our knowledge this appears to be the first time this has been documented and investigated. In contrast, the direct impact of bias-correcting input SST/SIC (versus not) has been investigated more thoroughly (e.g. Hoffmann et al., 2016). Enhanced high elevation warming is not the driver of this difference, noting that high elevation warming is more pronounced in winter (instead of summer). Instead, one possible explanation for this result is that the regional atmospheric circulation associated with warmer temperatures over New Zealand (i.e. more northerly flow conditions and/or more stable high-pressure ridging) tends to be enhanced into the future in the SST/SIC-driven simulations relative to the host GCM. In contrast, the nudged simulations will have trends in atmospheric circulation that are nearly identical to the GCM, due to the way the spectral nudging is performed.

Indeed, evidence directly supporting this is presented in Supplementary Material Figs. S2–S4. For each of the SST/SIC-driven CCAM simulations, the downscaled simulations across summer months tend to enhance ridging over New Zealand or to the east of New Zealand (shown in the MSLP projections) which drives more northerly flow conditions directly over New Zealand (indicated by the negative change in meridional flow [v850]). These northerly flow conditions are well known drivers of warmer conditions across New Zealand (Dean and Stott, 2009). These conditions are most pronounced in the downscaled projections from CNRM-CM6-1 and GFDL-ESM4. As shown in the near surface air temperature changes across the much wider South Pacific region (top row, Supplementary Material Figs. S2–S4), as expected, these regional circulation changes impact the enhanced warming only on a regional basis (i.e. over New Zealand) whereas the downscaled simulations have a much more similar warming rate to the driving GCM when averaged over this wider South Pacific region. The magnitude of the bias correction on climatological SST fields in the CCAM simulations is further shown in Supplementary Material Figs. S5–S6. As shown, bias correction tends to increase SSTs slightly on the western coasts of New Zealand and decrease SSTs on the eastern coasts. Notably, these differences around New Zealand remain consistent across both the historical and future periods, hence they cannot directly explain the change in warming over New Zealand.

3.2. *Mean precipitation*

Projections for mean precipitation are explored in Fig. 4. Here magenta shading is used to detail model projection uncertainty, based on sign agreement of the change across the ensemble. As before, projections are presented separately for the RCM (CCAM) and GCM ensemble to highlight how downscaling modifies the change patterns. For the RCM ensemble, the largest model agreement is typically seen in winter months. In winter, projections are for relatively large increases on the west coast of the South Island, exceeding 20 % in some places, accompanied by drying in the eastern and northern parts of both islands. A 20 % increase would be substantial for the west coast, given that observed annual rainfall can exceed 10 m in parts of this region, with total rainfall fairly consistent across seasons (Macara, 2016). The GCMs for winter show a similar overall spatial pattern, though the drying on the east coast of both islands is substantially reduced.

Despite using different RCMs and GCMs, this overall spatial pattern of precipitation change is generally similar to that reported from previous CMIP5 downscaling (MfE et al., 2008). As described in Gibson et al. (2024b), this overall spatial pattern is related to the intensification

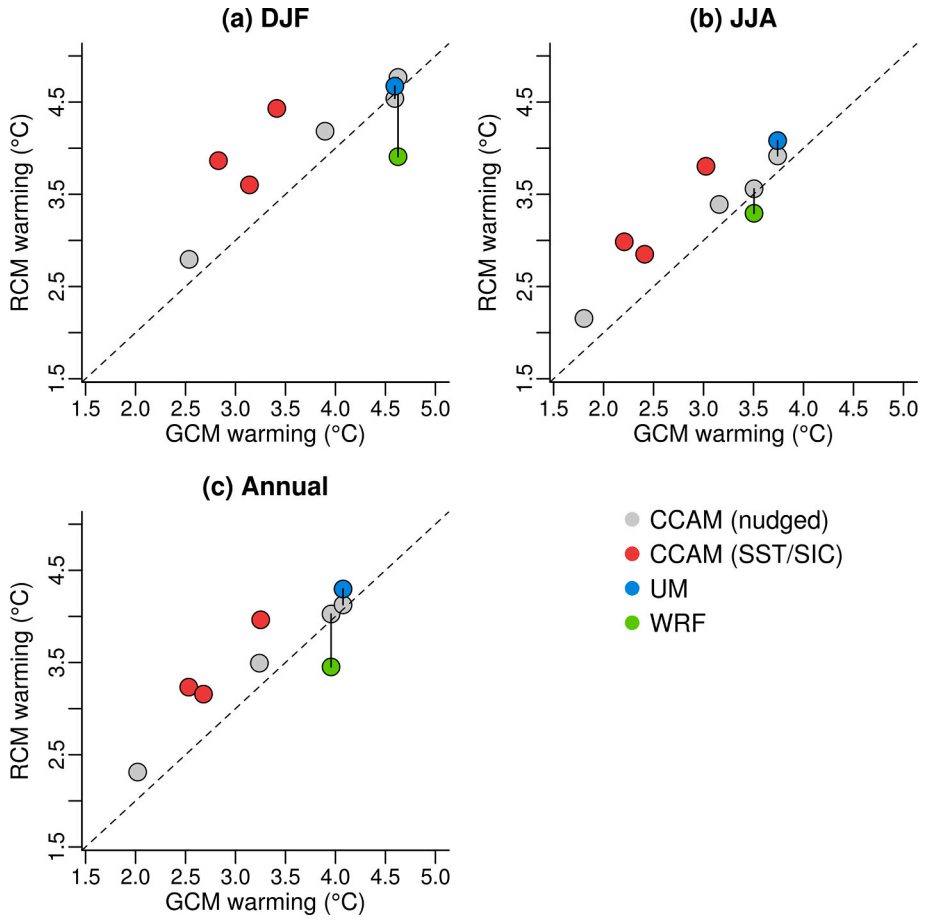

Fig. 3. Comparison of GCM (x-axis) and RCM (y-axis) projected warming (years 2080–2099 minus years 1986–2005) for daily maximum temperature (tasmax) under SSP370 averaged over New Zealand land-based grid cells. Different RCM configurations are shown according to colour. Solid vertical lines join (i.e. compare) different RCM warming responses for a given GCM, where available (see Table 1).

and southward shift of the jet, while the far north (i.e. of the North Island) drying appears related to shifts in Hadley cell extent which can differ between GCMs. Given the intensification of the jet, the enhanced drying on the east coast of the South Island in CCAM (relative to the GCMs) is very likely related to the better representation of topography in the RCM which creates a rain shadow effect under westerly flow conditions. The spring season (i.e. SON) projections in the RCM ensemble are very similar spatially to the winter change patterns, suggesting similar changes across large-scale drivers. However, the magnitude of the precipitation reductions is generally more pronounced in spring across most regions.

Compared to winter, the summer (i.e. DJF) projections are considerably more uncertain in the downscaled projections in terms of sign agreement. For winter, 66 % (i.e. 4 of 6) of the models in the ensemble agree on the sign of the change across 93.5 % of the country compared to only 66.9 % of the country for summer (Fig. 4). In summer, the changes are also much more spatially heterogenous indicating a lack of consistency in the associated large-scale circulation drivers. This was previously documented in Gibson et al. (2024b) highlighting the substantially larger uncertainty in mean precipitation projections in summer across CMIP6 models, where the relative role of internal variability is large. Since this uncertainty appears largely driven by a lack of consistent and robust drivers of large-scale circulation, it is not surprising that the RCM projections for summer do not reduce this uncertainty. It is important to note, as discussed by Giorgi (2019), the value of downscaled projections should not be thought of as reducing overall uncertainty, since downscaling/RCM uncertainty is not negligible and can be an important component of the full uncertainty.

We further explore the role of RCM uncertainty in the context of winter mean precipitation projections in Fig. 5. We have focused primarily on winter as this has been identified as the season with generally the most consistent change pattern (Fig. 4), including in CMIP6 GCMs (Gibson et al., 2024b) and earlier climate downscaling studies MfE (2018). This analysis is also presented for the spring season in Supplementary Material Fig. S7. Even for the winter pattern, Fig. 5 shows that notable RCM uncertainty on smaller scales can remain. While the main themes of the change pattern remain (i.e. wetter on the west, drier to the north and east), uncertainties become more important when considering location-specific changes (i.e on the scale of individual towns/cities) and their magnitudes. Since each of these RCM pairs (CCAM vs WRF; CCAM vs UM) is driven by the same GCM, we can be confident that these differences across RCMs are mostly driven by differences in the smaller scale RCM physics themselves. For spring, the strong drying identified earlier across northern and eastern regions (Fig. 4) is also apparent in the WRF and UM RCMs, which can show an even larger drying pattern in places (Fig. S7).

While the importance of RCM uncertainty has been noted in CORDEX projections in other regions, including across Australia (Evans et al., 2021), Europe (Sørland et al., 2018; Giorgi, 2019), North America (Bukovsky and Mearns, 2020), and Africa (Paeth et al., 2011), it is the first time to our knowledge that it has been quantified for New Zealand. This highlights that future downscaling exercises for New Zealand (i.e. for CMIP7) would benefit from placing greater emphasis on sampling RCM uncertainty, by including additional RCMs across the so-called GCM/RCM matrix (Giorgi, 2019). Since the main limitation to filling in the GCM/RCM matrix is computational resources, the use of RCM

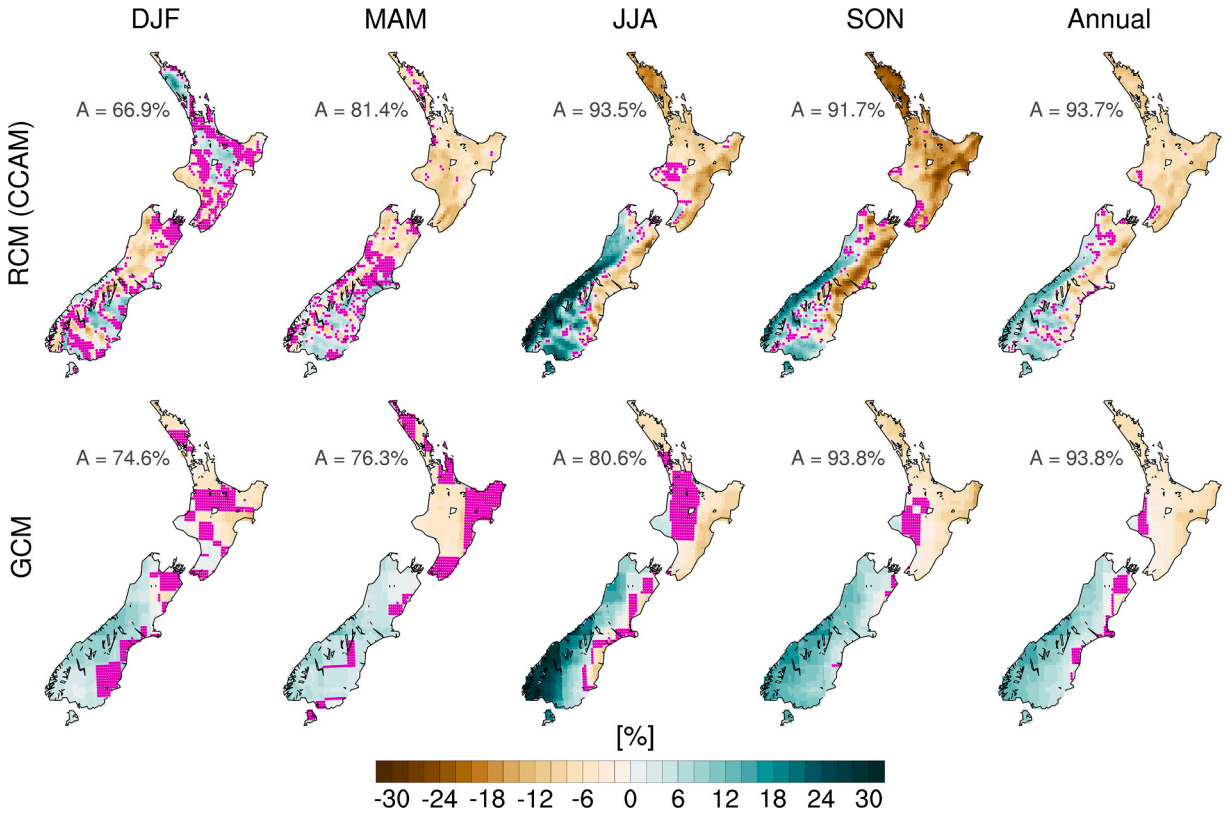

Fig. 4. Climate projections (years 2080–2099 minus years 1986–2005) under SSP370 for mean precipitation in each season. The top row shows the multi-model mean (n = 6) across RCMs (CCAM) and the bottom row shows the multi-model mean (n = 6) across the GCMs (i.e. prior to downscaling). Magenta shading indicates regions where there is less than 66 % agreement in the sign of the change across models, the 'A' value indicates the percentage of land area with non magenta shaded cells.

emulators based on machine learning (ML) and artificial intelligence (AI) could play an important role, alongside continued investment in dynamical regional models (Rampal et al., 2024; Evans et al., 2024). For building trust in AI-based projections, it will be important that both the historical biases and climate change patterns are carefully evaluated and understood alongside the dynamical models which they have been tasked with emulating (Rampal et al., 2024, 2025). Interpretable AI approaches, developed around process-based evaluation, could also help to build trust and community uptake (e.g. Gibson et al., 2021; Rampal et al., 2022). Additionally, exploring avenues for enhancing the RCM resolution beyond 12 km will be a focus of future work. Given the complex terrain of New Zealand, moving towards convection-permitting RCM resolutions (~2 km) will likely add further value in terms of more realistically representing orographic precipitation and precipitation extremes (Pirooz et al., 2023).

While scenario uncertainty was not the focus here, the downscaled projections for CCAM include three different scenarios (SSP126, SSP245, SSP370) which can be explored. The similarities and differences across scenarios for projections of mean precipitation is summarized in Fig. 6. To do so, the pattern correlation is computed between SSPs for different seasons and different downscaled models. As expected, the spatial patterns of change are overall more similar (i.e. higher pattern correlation) for comparing between SSP370 and SSP245 (Fig. 5b) than for SSP370 and SSP126 (Fig. 5a). The projections across SSPs are most consistent for JJA, SON (and annually). This finding generally agrees with findings in other regions globally, namely that when there is a robust and consistent climate change signal, the differences between SSPs mainly act to amplify the magnitude while preserving the spatial pattern (e.g. Neelin et al., 2013).

3.3. Temperature extremes

We begin by showing projections for several relatively simple temperature-based ETCCDI indicators followed by an analysis of heatwaves. Compared to the projections for daily mean temperature (Fig. 1), the ETCCDI indicators shown in Fig. 7 for the downscaled simulations (i.e. RCM) can show considerably larger changes in certain regional characteristics of extremes. This is especially apparent for TNn (annual minimum temperature) and number of frost days, indicating that the RCM (i.e. CCAM) warm the coldest extremes of the temperature distribution in the coldest regions more so than in the GCM. Given that these differences are clearly associated with elevation (i.e. more enhanced warming in the RCM in high elevation regions), it again seems likely that reduced snow cover and reduced albedo in winter months has contributed to this enhanced warming, again highlighting the added value of downscaling and improved representation of topography. Also notable is the enhanced diurnal temperature range in the downscaled simulations compared to the host GCM. This is related to the daily maximum temperatures generally warming faster than the daily minimum temperatures (hence widening the daily temperature range), with this finding generally consistent across regions and seasons (Supplementary Material Figs. S8–S10).

Before analysing future projections of heatwaves, the historical climatology (i.e. averaged over years 1986–2005) of heatwave metrics are presented in Supplementary Material Fig. S11. As represented in CCAM, the historical frequency and duration of heatwave days is relatively uniform across the country, as expected since heatwaves are defined based on the location-specific 95th percentiles. In particular, the average number of days per year belonging to a heatwave differs between 2 and 5 days, while the average duration is generally between 3 and 5 days. The amplitude, defined as the temperature on the hottest day

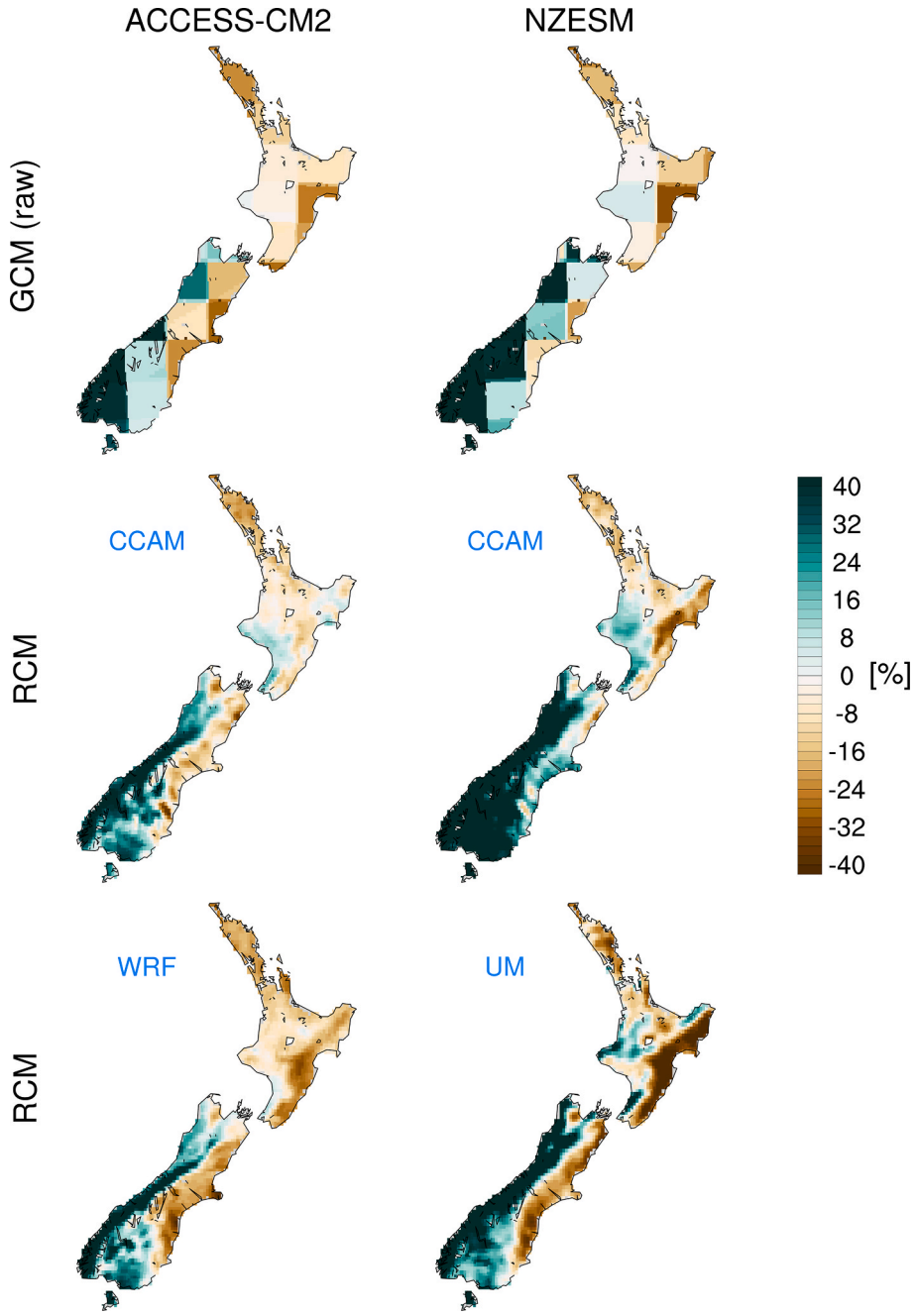

Fig. 5. Climate projections (years 2080–2099 minus years 1986–2005) under SSP370 for mean precipitation in winter (JJA) showing the sensitivity of the choice of RCM when downscaling ACCESS-CM2 and NZESM GCMs. ACCESS-CM2 is downscaled with CCAM and WRF; NZESM is downscaled with CCAM and UM.

of the hottest annual heatwave, shows much larger regional variation, as expected. The hottest heatwaves generally occur in eastern regions of the country over relatively flat terrain, often associated with foehn winds. These regional details in heatwave amplitude are clearly missing from the GCMs (bottom row of Fig. S11), again highlighting the added value of downscaling, as previously reported for the representation of hot extremes in Gibson et al. (2024a) and more broadly for heatwaves across Australia (Trancoso et al., 2020).

For downscaled projections of heatwaves (Fig. 8), large increases in heatwave frequency and duration are shown, particularly enhanced across the northern half of the North Island. These increases are substantial, going from a historical heatwave frequency of ~3 days per season to over 60 days in some regions. This corresponds to roughly 40 % of days per extended summer season (NDJFM) being classed as heatwaves, based on the historical 95th percentile 3-day definition of heatwaves. Similarly for duration, the average length of the longest duration heatwaves is projected to increase from 3 to 5 days to being multi-week events (i.e. exceeding 20 days in some regions). For heatwave amplitude, the downscaled projections show increases in the hottest days of between 3 and 5°C, broadly consistent with the projections shown earlier for TXx (single hottest day of year). The downscaled and GCM (raw) projections for heatwaves show similar overall patterns, especially for heatwave frequency and duration, while differences are larger for heatwave amplitude with the RCM ensemble showing larger increases in many regions.

These relatively large projected increases for heatwave frequency and duration are consistent with heatwave projections in other regions globally when similar levels of mean warming are reached (e.g. Cowan

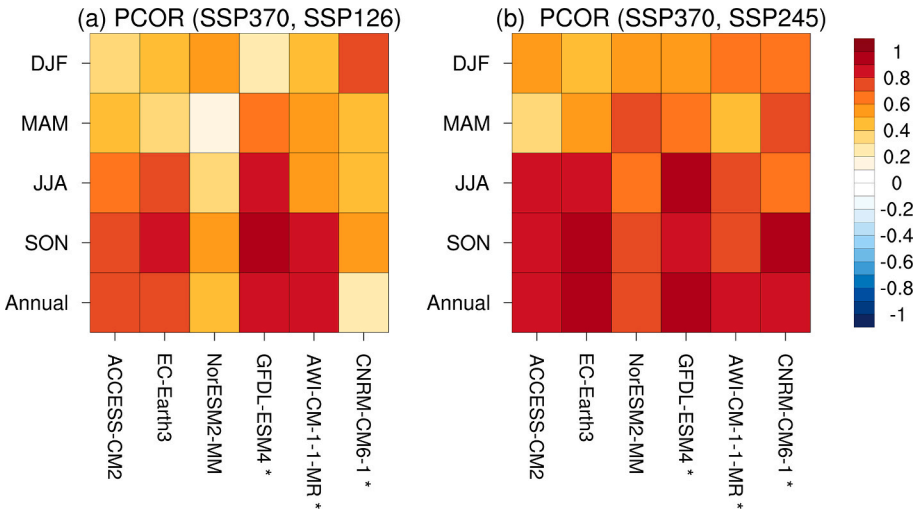

Fig. 6. Pattern correlation (PCOR) between select SSPs for different seasons and models for mean precipitation projections (years 2080–2099 minus years 1986–2005). Here each model refers to the CCAM downscaled output from that model.

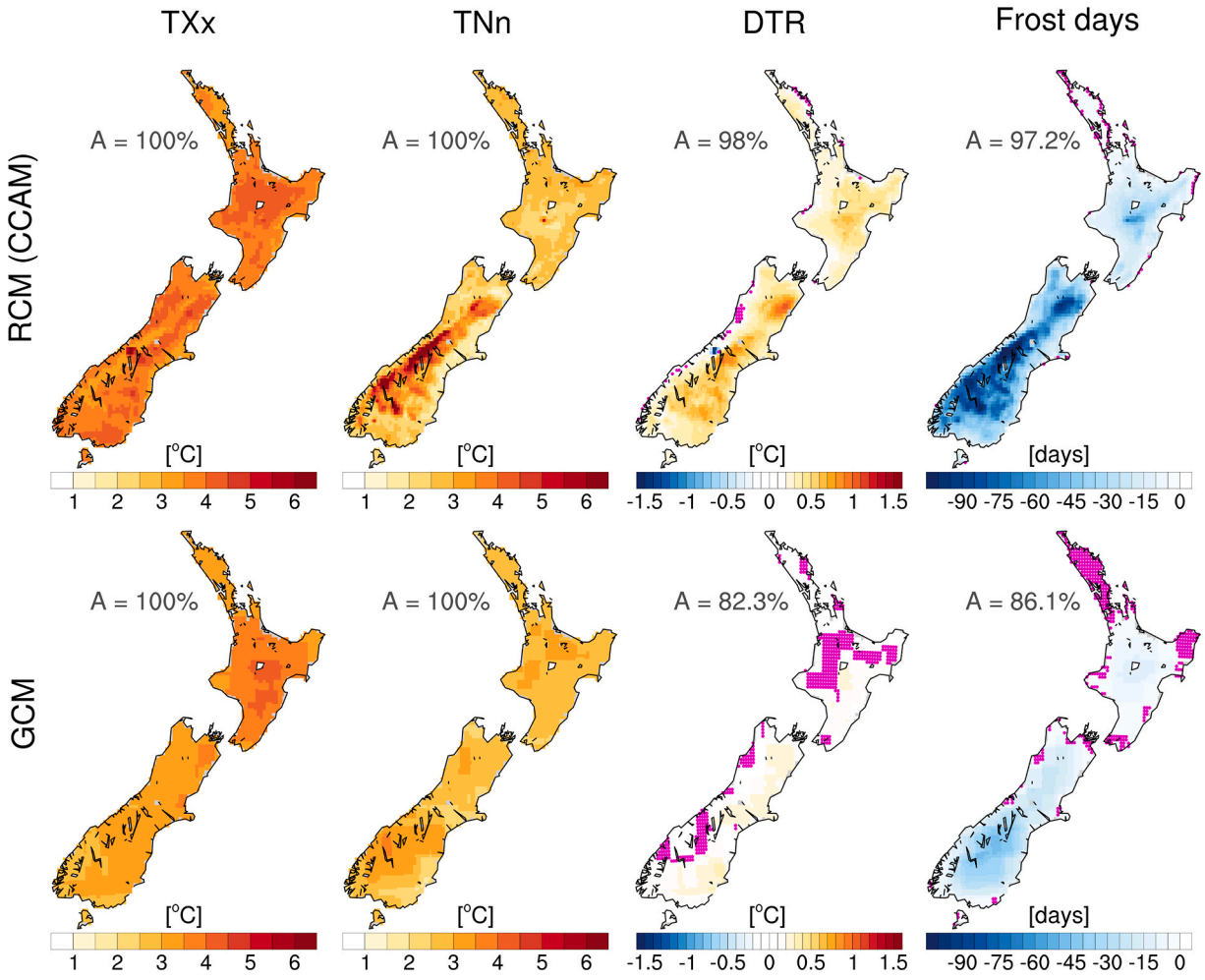

Fig. 7. Climate projections (years 2080–2099 minus years 1986–2005) under SSP370 for select temperature-based ETCCDI indices. The top row shows the multi-model mean (n = 6) across RCMs (CCAM) and the bottom row shows the multi-model mean (n = 6) across the GCM (i.e. prior to downscaling). Magenta shading indicates regions where there is less than 66 % agreement in the sign of the change across models, the 'A' value indicates the percentage of land area with non magenta shaded cells.

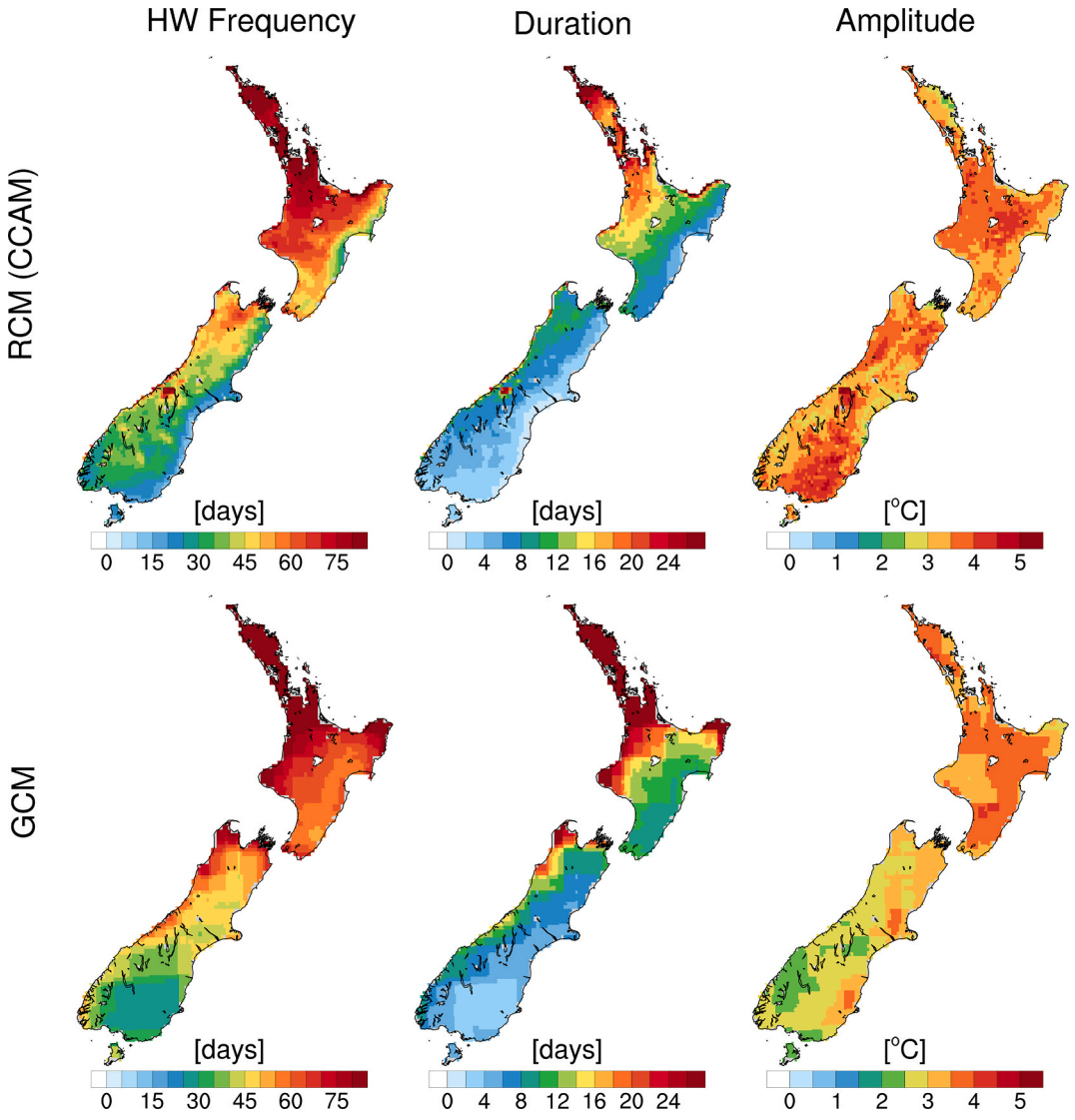

Fig. 8. Climate projections (years 2080–2099 minus years 1986–2005) under SSP370 for extended summer (months NDJFM) heatwave indices (frequency, duration, and amplitude). The top row shows the multi-model mean (n = 6) across RCMs (CCAM) and the bottom row shows the multi-model mean (n = 6) across the GCM (i.e. prior to downscaling). The corresponding heatwave indices for the historical climatology are shown in Supplementary Material Fig. S11.

et al., 2014; Perkins-Kirkpatrick and Gibson, 2017). For example, at +3°C warming, Perkins-Kirkpatrick and Gibson (2017) report heatwave frequency increases of between 40 and 120 heatwave days annually, with large regional differences across the globe. As described therein, regions with relatively low historical variability in daily maximum temperatures (i.e. the tropics and parts of the sub-tropics) show much larger increases in heatwave frequency and duration for a given warming level, which can somewhat complicate the practical interpretation of these changes. This contributes to why the northern parts of New Zealand show the largest projected increases in heatwave frequency and duration (Fig. 8), despite showing similar increases in summer tasmax (Fig. S9) and TXx (Fig. 7) to other regions across the country. As shown in Supplementary Material Fig. S12, these northern regions are those with the lowest historical variability in daily maximum temperatures, with this evident in both gridded observations and the downscaled output.

The change in TXx relative to the change in mean temperature (tas) is shown for each downscaled GCM (downscaled with CCAM) in Fig. 9. This change ratio shows how much faster the warm extremes (temperature tails) are projected to increase compared to the overall mean temperature. As shown in the multi-model mean of the downscaled ensemble, there is generally agreement that the tails are projected to warm faster than the mean (i.e. as indicated by TXx/tas >1). However, closer inspection of individual models and regions reveals important regional differences. There is some indication, in at least four of the downscaled models, that parts of the central North Island may show a "hotspot" for this change. Parts of Southland (the southernmost region of the South Island) is another region that stands out for the largest increases across models. When comparing across RCMs (CCAM, WRF, UM) for downscaling select GCMs (Fig. 10) regional differences in these hotspot regions are also apparent. This result highlights that the regional uncertainty in this ratio is driven both by differences in the driving fields from the GCM (as shown in Fig. 9) and by differences in the smaller scale RCM physics parameterizations (as shown in Fig. 10), including land-atmosphere interactions, and possibly by differences in the RCM ancillary files (e.g. land use, vegetation, soil properties).

Other studies, mostly focused on parts of North America and Europe, have used this ratio of TXx/tas in the context of studying land-atmosphere feedbacks in enhancing (or dampening) projected trends in temperature extremes (Seneviratne et al., 2016; Donat et al., 2017, 2018; Vogel et al., 2017). Future processed-based studies could extend our analysis to better understand and evaluate the role of soil moisture

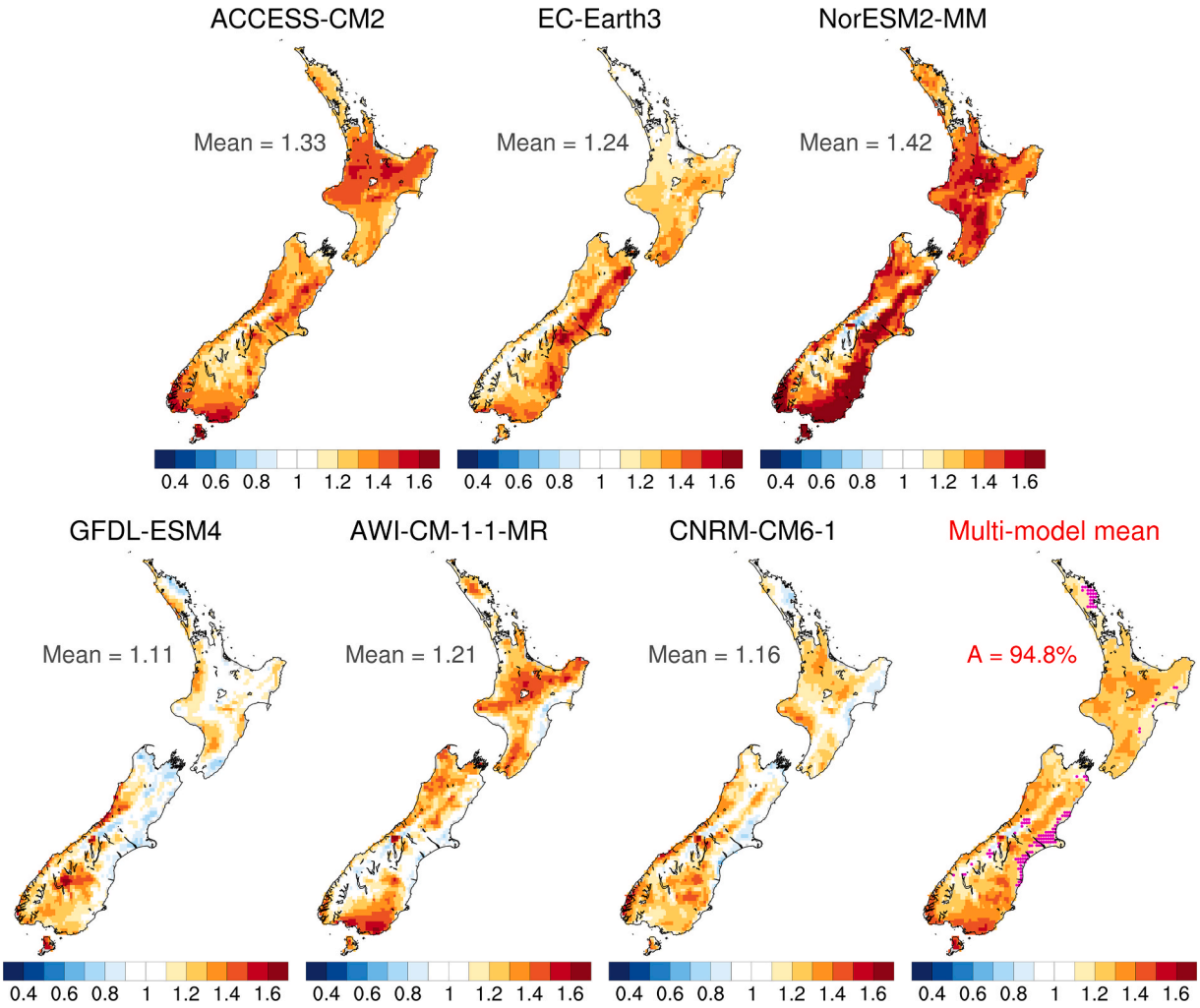

Fig. 9. Ratio of annual TXx/tas climate projections (years 2080–2099 minus years 1986–2005) under SSP370, where each model has been downscaled by CCAM. Positive values indicate that TXx is warming faster than tas, where TXx and tas are both defined locally (i.e. at each grid cell). The values in the top left of each panel are for the NZ-averaged change. Magenta shading indicates regions where there is less than 66 % agreement in the sign of the change across models, here defined as greater or less than 1. The agreement value (A) indicates the percentage of land area with non magenta shaded cells.

and surface fluxes across the different GCMs/RCMs and their influence on regional climate projections of temperature extremes for New Zealand (Harrington, 2021). Given our finding that regional differences in TXx/tas projections can stem from both GCM and RCM uncertainty, changes in cloudiness and circulation regimes (e.g. Gibson et al., 2017; Vautard et al., 2023) and land surface model uncertainty all likely play an important role, warranting further analysis for this understudied region.

3.4. *Precipitation extremes*

Climate projections for selected precipitation extremes from the ETCCDI indices is shown in Fig. 11. The annual number of wet days (>1 mm, R1mm) is projected to decrease in the downscaled simulations across most of the country, with the largest decreases widespread across the North Island. The downscaled projections for annual wet days closely resemble the overall spatial pattern of change from the raw GCM output. While the number of wet days is decreasing, the average precipitation rate on wet days (SDII) and the extreme precipitation rates (Rx1day and Rx3day) are both increasing, consistent with expectations from the thermodynamic drivers of precipitation extremes with warming (Trenberth, 2011; Pfahl et al., 2017; Fowler et al., 2021). Furthermore, the extremes are projected to increase faster than the mean precipitation increase on wet days. This implies that even where total annual precipitation is not projected to increase, the mean and extreme precipitation rates will increase but occur across fewer and shorter duration events, as also indicated by the general decrease in consecutive wet days (CWD).

As discussed in Harrington et al. (2024), this highlights the need to consider both the wet and dry extreme tails of the precipitation projections, as these changes can be masked when considering projections of total annual precipitation alone. Further analysis of this is provided in Fig. 12, showing changes in different quantiles of the daily precipitation distribution at select locations. As shown, even at locations where the total annual precipitation is projected to decrease (e.g. Gisborne, Auckland) the most extreme upper quantiles of the distribution (i.e. 0.99 and 0.999 quantiles) can still show pronounced projected increases at these locations.

For extreme precipitation indices, the projections from the raw GCM output are broadly consistent with the downscaled output, at least in terms of the change magnitude at the national scale. This is despite relatively large historical biases in the GCM output for a number of these indices, as documented in Gibson et al. (2024a). However, across finer regional scales, certain differences are notable. For the annual number of wet days (R1mm) the downscaled projections are more clearly impacted by terrain, especially over the South Island where the reduction in dry days is amplified in the lee of the Southern Alps. Since the topography is poorly represented in the GCMs, these changes are not

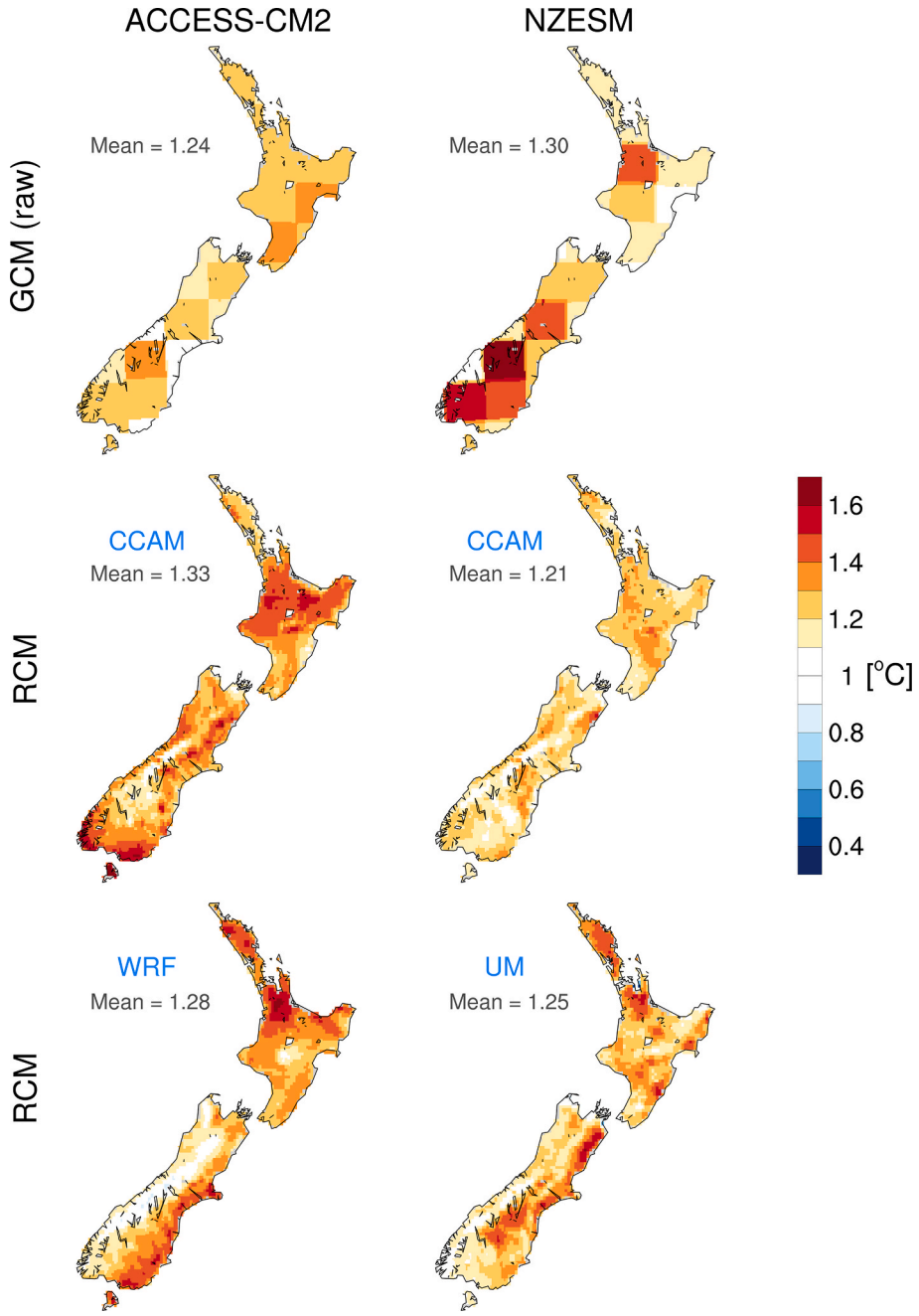

Fig. 10. Ratio of annual TXx/tas climate projections (years 2080–2099 minus years 1986–2005) under SSP370, showing the sensitivity of the choice of RCM when downscaling ACCESS-CM2 and NZESM GCMs. The values in the top left of each panel are for the NZ-averaged change. ACCESS-CM2 is downscaled with CCAM and WRF; NZESM is downscaled with CCAM and UM. The ACCESS-CM2 downscaled by CCAM projection panel is identical to that in Fig. 9.

well accounted for, highlighting the benefits of downscaling here. Furthermore, the downscaled simulations generally show much larger increases in the wettest annual events (Rx1day and Rx3day) across the top half of the North Island, which can exceed 20 %. Precipitation extremes in this region are often caused by ex-tropical cyclones, and associated atmospheric rivers, which are generally much better represented in the downscaled simulations relative to the raw GCMs (Gibson et al., 2024a). Differences in these driving processes may have contributed to the differences in the RCM versus GCM projections here. In terms of projection uncertainty, compared to the GCMs, the downscaled simulations can show slightly higher levels of uncertainty when expressed as a fraction of agreement across New Zealand (i.e. lower *A* values in Fig. 11) for certain indices (e.g. SDII, CWD), which may be related to the greater spatial detail provided by the RCM.

3.5. *Meteorological drought*

Climate projections for meteorological drought are shown in Fig. 13. The extended summer period (NDJFM) is shown here, while the change across individual downscaled GCMs is shown in Supplementary Material Figs. S13–15 for the same season. For drought frequency, relatively large increases (>50 %) in the number of events is projected across the models over large parts of the northern and eastern regions of both islands. For projections of drought frequency, there can be large differences between the RCM and raw GCM output. As discussed earlier, the better representation of topography is apparent in the RCM change patterns, driving the west/east gradient in the response across the South Island that is not captured in the GCMs. Another notable difference is the overall larger increase in drought frequency over the North Island in the downscaled

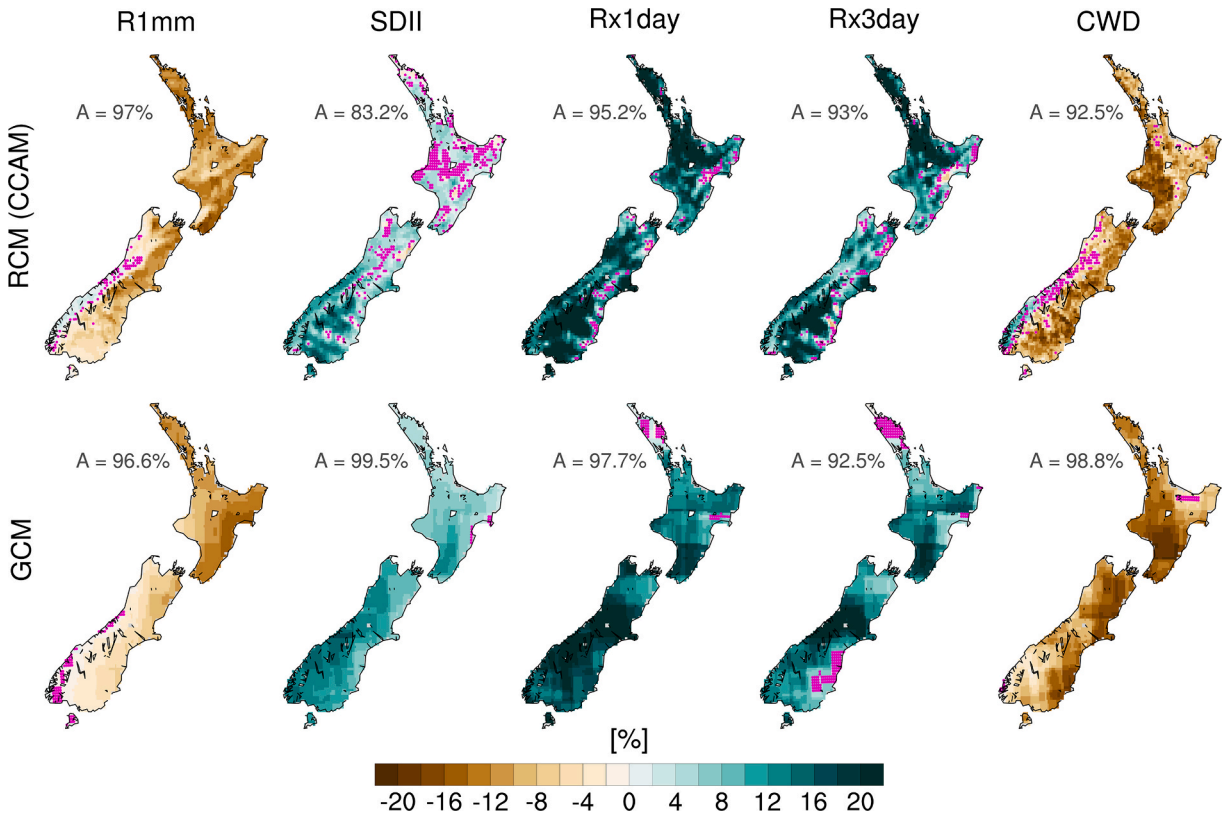

Fig. 11. Climate projections (years 2080–2099 minus years 1986–2005) under SSP370 for select precipitation based ETCCDI indices. The top row shows the multi-model mean (n = 6) across RCMs (CCAM) and the bottom row shows the multi-model mean (n = 6) across the GCM (i.e. prior to downscaling). Magenta shading indicates regions where there is less than 66 % agreement in the sign of the change across models, the 'A' value indicates the percentage of land area with non magenta shaded cells.

output compared to the raw GCM. It appears both large-scale circulation conditions and smaller scale RCM physics play a role in driving this. For example, as shown in Fig. S13, there are reasonably large differences across the individual downscaled CCAM simulations at regional scales, with the SST-driven simulations showing the largest increases in drought frequency across this region and season. Extending beyond the simple circulation projections shown earlier (Supplementary Material Figs. S2–S4), further detailed process-based analysis of these downscaled simulations would be useful, targeting both differences and trends in large-scale circulation patterns (i.e. blocking) relevant to drought, and smaller scale land-atmosphere feedbacks that can promote drying trends.

The projections for downscaled drought duration and intensity generally align with drought frequency projections. Namely, the largest and most consistent projected increase in drought duration and intensity are across the north and east regions of both islands. When comparing the uncertainty in projections across downscaled models, it is notable that the projections for summer drought statistics (Fig. 13) are more consistent (i.e. lower uncertainty) than projections for summer mean precipitation (Fig. 4). For example, when sign agreement is defined at the 66 % level (i.e. 4 of 6 models) there is agreement for mean precipitation change across only ~67 % of the country, compared to ~90 % of the country for drought intensity. As such, for regions of the country where the summer mean precipitation change is highly uncertain, more confident statements around drought statistics may still be possible for this same region. The explanation for this is that the processes driving mean precipitation can differ from those driving meteorological drought, with the latter also impacted considerably by future changes in long-term precipitation variability (Sheffield and Wood, 2012; Ukkola et al., 2020). This finding, that projected changes in meteorological drought statistics are generally more consistent and robust than for mean precipitation, was reported and discussed in Ukkola et al. (2020) for multiple other global land regions from GCMs.

Despite differences in the models (both GCMs and RCM), and the approach for defining drought, the projections reported here for meteorological drought are broadly consistent with those from previous CMIP5 downscaled projections for New Zealand MfE (2018). Namely, previous downscaled projections also emphasized the largest increases in drought frequency and severity across northern and eastern regions of both islands, which are climatologically dry areas. Here we adopt a simpler meteorological drought definition (i.e. a sustained deficit of precipitation) compared to previous approaches that used offline calculations of potential evapotranspiration (PET) in combination with an offline water balance model to define potential evapotranspiration deficits (PED). While each approach can be useful in certain contexts, we suggest that the simpler meteorological drought approach adopted here has a number of benefits. When used in a climate change context, recent studies have expressed concern that offline use of PET may overestimate future drought, including through potentially 'double-counting' important feedbacks on surface humidity and temperature (Swann et al., 2016; Yang et al., 2019; Ukkola et al., 2020). Furthermore, it is a difficult task for state-of-the-art RCMs to faithfully represent all variables that go into calculations of PET. Indeed, as discussed in MfE (2018), previous projections of PET/PED were considered preliminary given the relatively large disparities between the model historical climatology for these quantities and observational estimates, while noting that observational estimates also have a relatively high degree of uncertainty.

3.6. Summary of projection uncertainty

For the climate projections presented earlier, uncertainty estimates were assigned based on model sign agreement computed across the

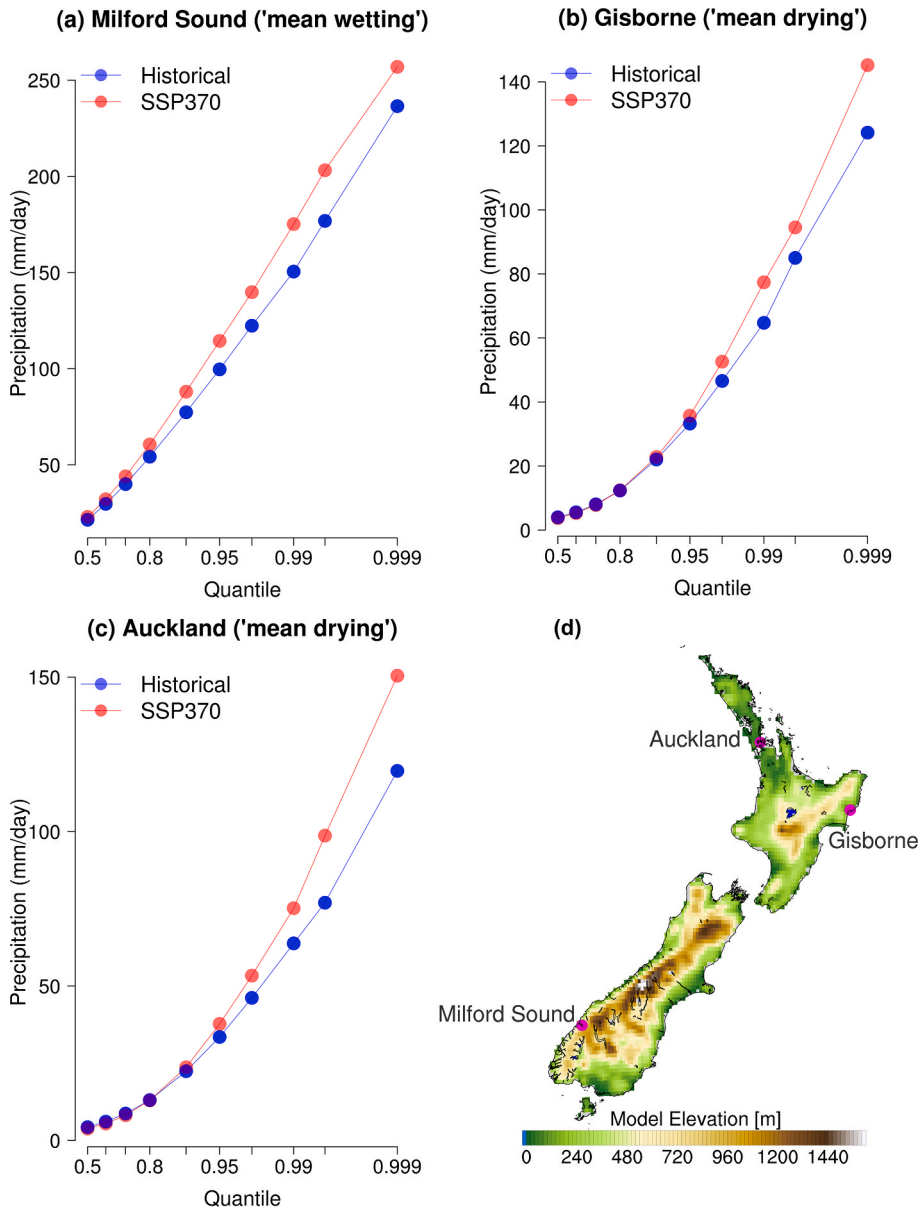

Fig. 12. Daily precipitaiton at different quantiles of the distribution for historical (years 1986–2005) and SSP370 (years 2080–2099) from the CCAM RCM ensemble. Three example locations are shown based on 'mean wetting' (panel a) and 'mean drying' (panel b and c) from the mean annual precipitation projections shown earlier in Fig. 4.

country (e.g. Fig. 4). In those figures, agreement was defined based on 4 of 6 model (i.e. >66 %) sign agreement threshold. In Fig. 14, we present a summary of these findings across indices and seasons, as well as testing the sensitivity to a stricter threshold for model agreement (i.e. 5 of 6 models, >83 %). For the sake of brevity, we only present precipitation-based indices/variables, given that most temperature-based indices/variables analysed have complete agreement (i.e. 100 %). As discussed earlier, projections of the meteorological drought statistics for summer (i.e. frequency, duration, intensity) are more consistent than for summer mean precipitation, and this finding holds across both thresholds of model agreement. Similarly, extreme precipitation indices (i.e. Rx1day/Rx3day) are more consistent than annual mean precipitation projections. Projections of mean precipitation in winter (JJA) are also more consistent than for summer (DJF), as discussed earlier this is likely related to more robust large-scale circulation trends in winter across the models.

As discussed in Gibson et al. (2024b), for projections of summer mean precipitation over New Zealand, it appears it will be difficult to further constrain this uncertainty, given the apparent role of internal variability which is enhanced in this season even under a high emissions scenario. As such, for climate adaptation and planning purposes, it may be more appropriate to focus on projections of the tails of the distribution (i.e. heavy precipitation extremes or drought) where confidence is larger, or to communicate a storylines approach for defining risk (Shepherd et al., 2018; Narsey et al., 2022; Gibson et al., 2024b) based on different physically plausible pathways describing how these quantities may change regionally into the future. Ongoing efforts to improve RCM resolution towards convection-permitting scales over New Zealand will likely also further improve the representation of precipitation extremes and related processes (Pirooz et al., 2023; Campbell et al., 2024).

4. Conclusions

Downscaled climate projections provide high-resolution information important for planning and climate adaptation purposes, which is not readily available from GCM output directly. In terms of providing

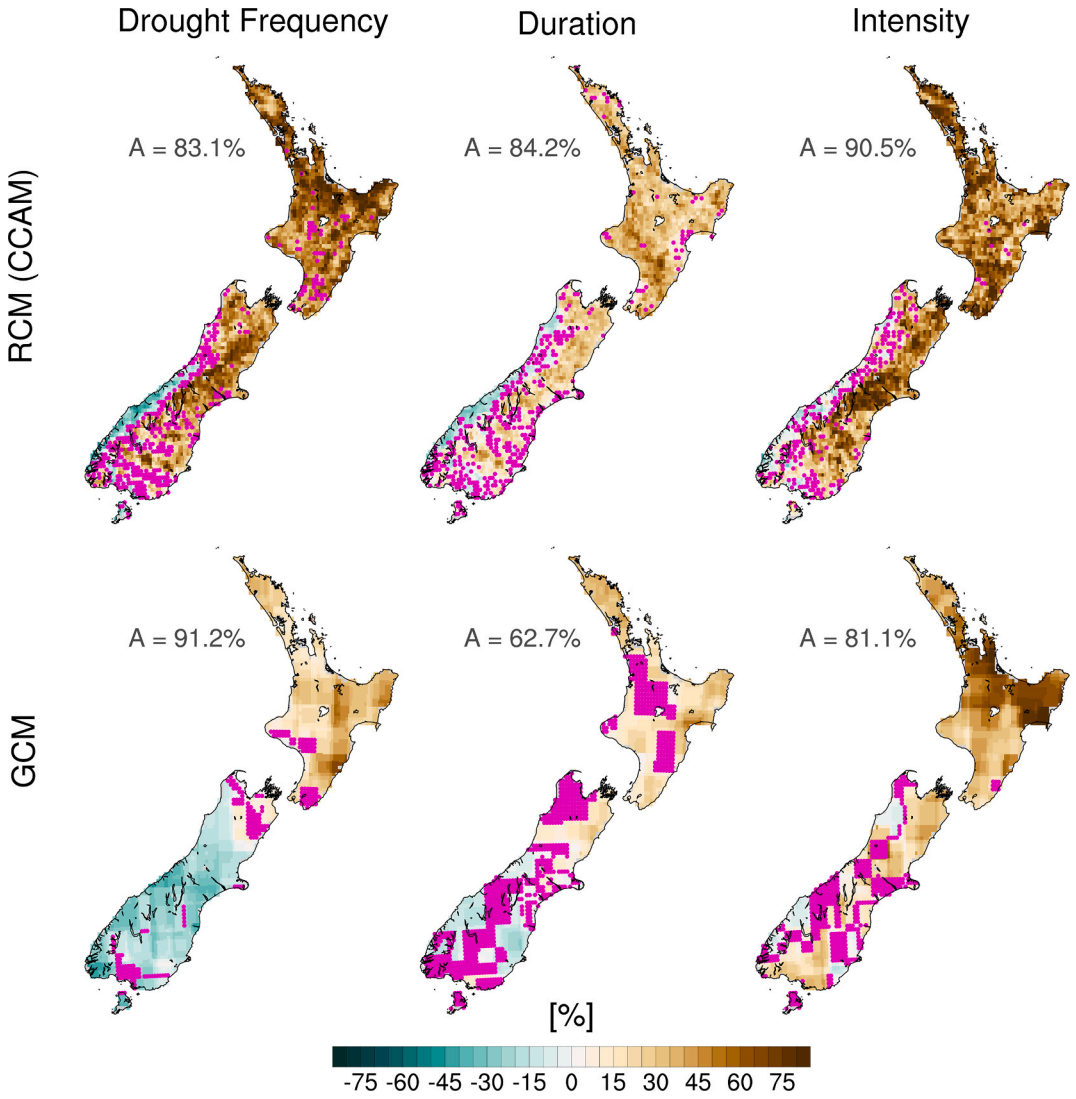

Fig. 13. Climate projections (years 2080–2099 minus years 1986–2005) under SSP370 for summer (months NDJFM) meteorological drought indices (frequency, duration, and intensity). The top row shows the multi-model mean (n = 6) across RCMs (CCAM) and the bottom row shows the multi-model mean (n = 6) across the GCM (i.e. prior to downscaling). Magenta shading indicates regions where there is less than 66 % agreement in the sign of the change across models, the 'A' value indicates the percentage of land area with non magenta shaded cells.

century-long projections from a range of GCMs and emissions scenarios, the updated projections presented here encompass the highest-resolution ensemble of physics-based model projections for New Zealand to date. Focusing on a relatively high emissions scenario (SSP3-7.0), a summary of some of the main findings from these updated CMIP6 projections are:

- Daily maximum temperatures are generally projected to increase faster than daily minimum temperatures, with the largest projected increases in summer. This leads to projected increases in daily temperature range across most of the country. In general, high-elevation regions warm the most. These findings are qualitatively consistent with earlier CMIP5 projections.
- For mean precipitation, the most consistent projections are for winter and spring, associated with a wetting response on the west and south of New Zealand and drying to the north and east. Model projections diverge more considerably for summer mean precipitation projections. At a regional to national scale, these broad patterns of change and seasonal variability are generally consistent with earlier CMIP5 projections.
- Downscaling tends to enhance the overall warming from the GCMs. This can differ between RCMs and differ depending on how the RCM is driven by the GCM (i.e. whether driven by spectral nudging or driven in AMIP mode from SST/SIC fields). The differences are largest for daily maximum temperatures in summer.
- Although the winter mean precipitation projections are the most consistent of any season, at smaller scales and in some regions, differences can arise when comparing different RCMs driven by the same GCM.
- Compared to the projections from GCMs which lack important orography, downscaling adds considerable detail for certain extreme temperature indices. Most notably, larger increases in high elevation regions are evident for the warming of cold-tail temperature extremes (i.e. TNn). Similarly, the projected decease in frost days with warming is much more pronounced, highlighting a key aspect of added value from downscaling.
- Summer heatwave projections from the downscaled simulations indicate relatively large increases in frequency, duration and amplitude (3–5°C warmer) towards the end-of-century, particularly for the northernmost regions of the country. The warm tail of the temperature distribution generally warms faster than the mean,

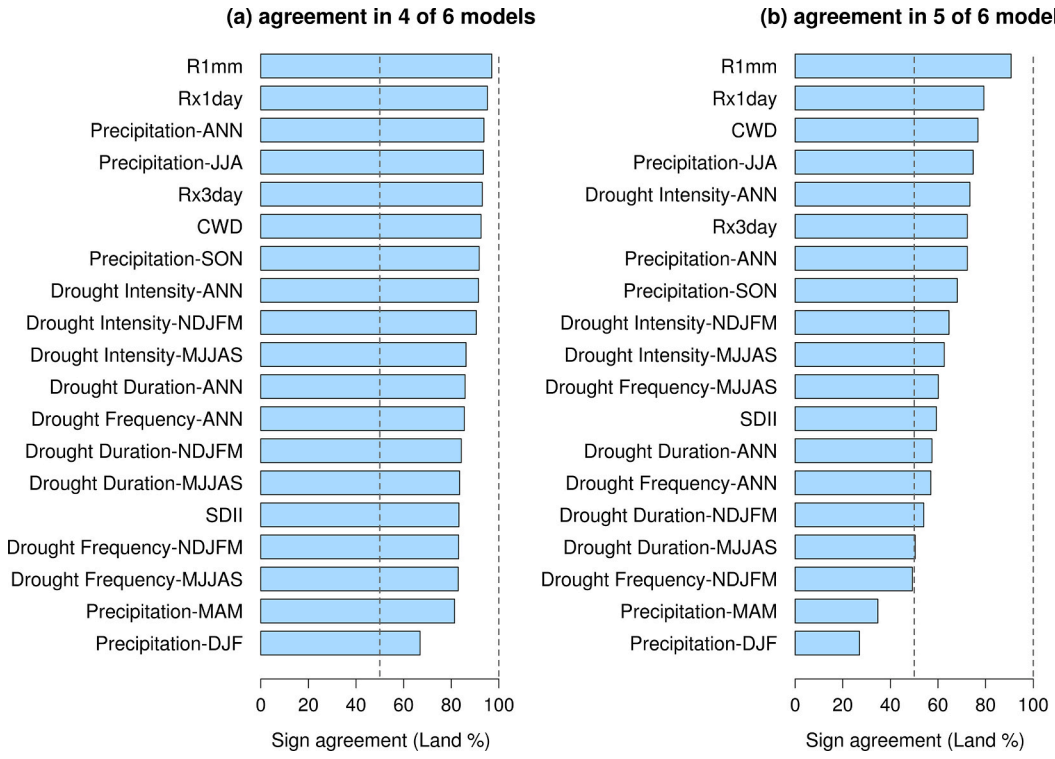

Fig. 14. Summary of the sign agreement over land for climate projections across models for different precipitation-based indices/seasons. Panel a shows agreement when defined as being greater than ~66 % sign agreement across models (i.e. 4 of 6), panel b shows agreement when defined as being greater than ~83 % sign agreement across models (i.e. 5 of 6).

consistent across most regions and downscaled models. However, the rate at which this occurs differs regionally between models, requiring further investigation into the relevant driving processes across scales.

- Consistent with expectations from thermodynamic drivers of extreme precipitation, the largest relative projected increases are in the tails of the distribution (i.e. Rx1day increases faster than the mean). Across most regions, the number of wet days is also projected to decrease, indicating more extreme precipitation spread across fewer and shorter duration periods. An exception to this is for the west coast of the South Island, where all precipitation indicators increase, likely further enhanced by dynamical drivers (Gibson et al., 2024b).
- A summary of uncertainty is presented based on quantifying the percentage of land area where there is sign agreement across the models. Given the importance of thermodynamic drivers, projections of precipitation extremes have greater model agreement than mean precipitation. Similarly, projections of drought in summer have greater model agreement than summer mean precipitation.

By covering a wide range of projections here, including various extreme indices, we anticipate that this will provide a useful foundation for future impact and adaptation studies. The uncertainty metrics provided will help users of the model projections better understand where the largest uncertainties lie in terms of the direction of change. Lastly, we have shown that RCM uncertainty can be non-negligible for certain regions and variables/indicators, which has been historically understudied. Improved sampling of uncertainty, stemming from both GCM and RCM uncertainty, would require significantly larger computational resources than currently allocated. To address this, one avenue currently being explored is the extent to which AI-based RCM emulators can alleviate some of this computational burden, while still providing scientifically credible projections (Rampal et al., 2024, 2025).

CRediT authorship contribution statement

Peter B. Gibson: Writing – original draft, Visualization, Methodology, Investigation, Formal analysis, Data curation, Conceptualization. **Ashley M. Broadbent:** Writing – review & editing, Methodology, Data curation, Conceptualization. **Stephen J. Stuart:** Writing – review & editing, Methodology, Data curation, Conceptualization. **Hamish Lewis:** Methodology, Formal analysis, Data curation, Conceptualization. **Isaac Campbell:** Methodology, Conceptualization. **Neelesh Rampal:** Writing – review & editing, Methodology, Conceptualization. **Luke J. Harrington:** Writing – review & editing, Methodology, Investigation, Conceptualization. **Jonny Williams:** Writing – review & editing, Data curation.

Code availability

The heatwave analysis code was produced by Tammas Loughran https://github.com/tammasloughran/ehfheatwaves. The CCAM source code is available from CSIRO https://bitbucket.csiro.au/projects/CCAM/repos/ccam/browse.

Declaration of competing interest

The authors declare that they have no known competing financial interests or personal relationships that could have appeared to influence the work reported in this paper.

Acknowledgements

We acknowledge the World Climate Research Programme, which, through its Working Group on Coupled Modelling, coordinated and promoted CMIP6. We thank the climate modelling groups for producing and making available their model output, the Earth System Grid Federation (ESGF) for archiving the data and providing access, and the

multiple funding agencies who support CMIP6 and ESGF. We thank Marcus Thatcher (CSIRO) for technical assistance and guidance with CCAM, and Dáithí Stone for providing feedback on an earlier version of the manuscript.

Funding for this work has been provided by New Zealand's Ministry for Business, Innovation and Employment (MBIE)'s Building for Climate Change programme and is contracted through the Ministry for the Environment (MfE contract number 25679). The work is also supported by MBIE Strategic Science Investment funding (contract number C01X1703). Authors PBG, HL, LJH received funding from Marsden Grant MFP-UOW2307.

Appendix A. Supplementary data

Supplementary data to this article can be found online at https://doi.org/10.1016/j.wace.2025.100784.

Data availability

The CMIP6 output is available from the Earth System Grid Federation (ESGF) archive: https://esgf-node.llnl.gov/projects/cmip6/. Information about how to access the CCAM downscaled output used in this study is available through: https://niwa.co.nz/climate/research-projects/updated-national-climate-projections-for-aotearoa-new-zealand.

References

Ackerley, D., Dean, S., Sood, A., Mullan, A.B., 2012. Regional climate modelling in New Zealand Comparison to gridded and satellite observations. Weather Clim. 32 (1), 3–22. https://doi.org/10.2307/26169722.

Akhter, M.S., Shamseldin, A.Y., Melville, B.W., 2019. Investigation of climate change impacts on flow regime in the Lucas Creek catchment using multiple CMIP5 ensembles. Urban Water J. 16 (5), 389–401. https://doi.org/10.1080/1573062X.2019.1669199.

Behrens, E., Williams, J., Morgenstern, O., Sutton, P., Rickard, G., Williams, M.J.M., 2020. Local grid refinement in New Zealand's earth system model: tasman sea ocean circulation improvements and super-gyre circulation implications. J. Adv. Model. Earth Syst. 12 (7), e2019MS001996. https://doi.org/10.1029/2019MS001996.

Bi, D., Dix, M., Marsland, S., O'farrell, S., Sullivan, A., Bodman, R., Law, R., Harman, I., Srbinovsky, J., Rashid, H.A., 2020. Configuration and spin-up of ACCESS-CM2, the new generation Australian community climate and earth system simulator coupled model. J. South. Hemisphere Earth Syst. Sci. 70 (1), 225–251.

Bukovsky, M.S., Mearns, L.O., 2020. Regional climate change projections from NA-CORDEX and their relation to climate sensitivity. Clim. Change 162 (2), 645–665.

Campbell, I., Gibson, P.B., Stuart, S., Broadbent, A.M., Sood, A., Pirooz, A.A., Rampal, N., 2024. Comparison of three reanalysis-driven regional climate models over New Zealand: climatology and extreme events. Int. J. Climatol. 44 (12), 4219–4244.

Chapman, S., Syktus, J., Trancoso, R., Thatcher, M., Toombs, N., Wong, K.K.H., Takbash, A., 2023. Evaluation of dynamically downscaled CMIP6-CCAM models over Australia. Earth's future, 11 (11), e2023EF003548.

Collins, D.B., 2020. New Zealand river hydrology under late 21st century climate change. Water (Lond. 1974) 12 (8), 2175.

Cowan, T., Purich, A., Perkins, S., Pezza, A., Boschat, G., Sadler, K., 2014. More frequent, longer, and hotter heat waves for Australia in the twenty-first century. J. Clim. 27 (15), 5851–5871. https://doi.org/10.1175/JCLI-D-14-00092.1.

Dean, S., Stott, P., 2009. The effect of local circulation variability on the detection and attribution of New Zealand temperature trends. J. Clim. 22 (23), 6217–6229.

Donat, M.G., Pitman, A.J., Seneviratne, S.I., 2017. Regional warming of hot extremes accelerated by surface energy fluxes. Geophys. Res. Lett. 44 (13), 7011–7019. https://doi.org/10.1002/2017GL073733.

Donat, M.G., Pitman, A.J., Angélil, O., 2018. Understanding and reducing future uncertainty in midlatitude daily heat extremes via land surface feedback constraints. Geophys. Res. Lett. 45 (19), 10–627. https://doi.org/10.1029/2018GL079128, 610,636.

Drost, F., Renwick, J., Bhaskaran, B., Oliver, H., McGregor, J., 2007. Simulation of New Zealand's climate using a high-resolution nested regional climate model. Int. J. Climatol.: J. Royal Meteorol. Soc. 27 (9), 1153–1169.

Evans, J.P., Di Virgilio, G., Hirsch, A.L., Hoffmann, P., Remedio, A.R., Ji, F., Rockel, B., Coppola, E., 2021. The CORDEX-Australasia ensemble: evaluation and future projections. Clim. Dyn. 57, 1385–1401.

Evans, J.P., Belmadani, A., Menkes, C., Stephenson, T., Thatcher, M., Gibson, P.B., Peltier, A., 2024. Higher-resolution projections needed for small island climates. Nat. Clim. Change 14 (7), 668–670. https://doi.org/10.1038/s41558-024-02028-9.

Fiedler, T., Pitman, A.J., Mackenzie, K., Wood, N., Jakob, C., Perkins-Kirkpatrick, S.E., 2021. Business risk and the emergence of climate analytics. Nat. Clim. Change 11 (2), 87–94.

Fowler, H.J., Lenderink, G., Prein, A.F., Westra, S., Allan, R.P., Ban, N., Barbero, R., Berg, P., Blenkinsop, S., Do, H.X., Guerreiro, S., Haerter, J.O., Kendon, E.J., Lewis, E., Schaer, C., Sharma, A., Villarini, G., Wasko, C., Zhang, X., 2021. Anthropogenic intensification of short-duration rainfall extremes. Nat. Rev. Earth Environ. 2 (2), 107–122. https://doi.org/10.1038/s43017-020-00128-6.

Gibson, P.B., Pitman, A.J., Lorenz, R., Perkins-Kirkpatrick, S.E., 2017. The role of circulation and land surface conditions in current and future Australian heat waves. J. Clim. 30 (24), 9933–9948. https://doi.org/10.1175/JCLI-D-17-0265.1.

Gibson, P.B., Chapman, W.E., Altinok, A., Delle Monache, L., DeFlorio, M.J., Waliser, D. E., 2021. Training machine learning models on climate model output yields skillful interpretable seasonal precipitation forecasts. Commun. Earth Environ. 2 (1), 159.

Gibson, P.B., Stone, D., Thatcher, M., Broadbent, A., Dean, S., Rosier, S.M., Stuart, S., Sood, A., 2023. High-resolution CCAM simulations over New Zealand and the South Pacific for the detection and attribution of weather extremes. J. Geophys. Res. Atmos. 128 (14), e2023JD038530. https://doi.org/10.1029/2023JD038530.

Gibson, P.B., Stuart, S., Sood, A., Stone, D., Rampal, N., Lewis, H., Broadbent, A., Thatcher, M., Morgenstern, O., 2024a. Dynamical downscaling CMIP6 models over New Zealand: added value of climatology and extremes. Clim. Dyn. https://doi.org/10.1007/s00382-024-07337-5.

Gibson, P.B., Rampal, N., Dean, S.M., Morgenstern, O., 2024b. Storylines for future projections of precipitation over New Zealand in CMIP6 models. J. Geophys. Res. Atmos. 129 (5), e2023JD039664.

Giorgi, F., 2019. Thirty years of regional climate modeling: where are we and where are we going next? J. Geophys. Res. Atmos. 124 (11), 5696–5723.

Gonçalves, C., Honrado, J.P., Cerejeira, J., Sousa, R., Fernandes, P.M., Vaz, A.S., Alves, M., Araújo, M., Carvalho-Santos, C., Fonseca, A., 2022. On the development of a regional climate change adaptation plan: integrating model-assisted projections and stakeholders' perceptions. Sci. Total Environ. 805, 150320.

Grose, M.R., Narsey, S., Trancoso, R., Mackallah, C., Delage, F., Dowdy, A., Di Virgilio, G., Watterson, I., Dobrohotoff, P., Rashid, H.A., 2023. A CMIP6-based multi-model downscaling ensemble to underpin climate change services in Australia. Clim. Ser. 30, 100368.

Harrington, L.J., 2021. Rethinking extreme heat in a cool climate: a New Zealand case study. Environ. Res. Lett. 16 (3), 034030.

Harrington, L.J., Dean, S.M., Awatere, S., Rosier, S., Queen, L., Gibson, P.B., Barnes, C., Zachariah, M., Philip, S., Kew, S., 2023. The Role of Climate Change in Extreme Rainfall Associated with Cyclone Gabrielle over Aotearoa New Zealand's East Coast.

Harrington, L.J., Rosier, S.M., Marsh, T.I., Frame, D.J., 2024. Robust changes to the wettest and driest days of the year are hidden within annual rainfall projections: a New Zealand case study. Environ. Res. Lett. 19 (7), 074057. https://doi.org/10.1088/1748-9326/ad585a.

Hausfather, Z., Peters, G.P., 2020. Emissions–the 'business as Usual' Story Is Misleading. Nature Publishing Group.

Hausfather, Z., Marvel, K., Schmidt, G.A., Nielsen-Gammon, J.W., Zelinka, M., 2022. Climate simulations: recognize the 'hot model' problem. Nature 605 (7908), 26–29.

Hoffmann, P., Katzfey, J.J., McGregor, J.L., Thatcher, M., 2016. Bias and variance correction of sea surface temperatures used for dynamical downscaling. J. Geophys. Res. Atmos. 121 (21), 12–877. https://doi.org/10.1002/2016JD025383, 812,890.

Jakob, C., Gettelman, A., Pitman, A., 2023. The need to operationalize climate modelling. Nat. Clim. Change 13 (11), 1158–1160. https://doi.org/10.1038/s41558-023-01849-4.

Jobst, A.M., Kingston, D.G., Cullen, N.J., Schmid, J., 2018. Intercomparison of different uncertainty sources in hydrological climate change projections for an alpine catchment (upper Clutha River, New Zealand). Hydrol. Earth Syst. Sci. 22 (6), 3125–3142. https://doi.org/10.5194/hess-22-3125-2018.

Knutti, R., Masson, D., Gettelman, A., 2013. Climate model genealogy: generation CMIP5 and how we got there. Geophys. Res. Lett. 40 (6), 1194–1199. https://doi.org/10.1002/grl.50256.

Lee, J., Marotzke, J., Bala, G., Cao, L., Corti, S., Dunne, J., Engelbrecht, F., Fischer, E., Fyfe, J., Jones, C., A, Maycock, J.M., Ndiaye, O., S, Panickal, T., 2021. Zhou Future Global Climate: Scenario-Based Projections and Near-Term Information/Climate Change 2021: the Physical Science Basis. Contribution of Working Group I to the Sixth Assessment Report of the Intergovernmental Panel on Climate Change. Cambridge University Press, Cambridge, UK. https://doi.org/10.1017/9781009157896.006.

Lorrey, A.M., Griffiths, G., Fauchereau, N., Diamond, H.J., Chappell, P.R., Renwick, J., 2014. An ex-tropical cyclone climatology for Auckland, New Zealand. Int. J. Climatol. 34 (4).

Macara, G.R., 2016. *The climate and weather of West Coast.* NIWA. https://niwa.co.nz/sites/default/files/West_Coast_Climatology_NIWA_web.pdf.

Marotzke, J., Jakob, C., Bony, S., Dirmeyer, P.A., O'Gorman, P.A., Hawkins, E., Perkins-Kirkpatrick, S., Quéré, C.L., Nowicki, S., Paulavets, K., Seneviratne, S.I., Stevens, B., Tuma, M., 2017. Climate research must sharpen its view. Nat. Clim. Change 7 (2), 89–91. https://doi.org/10.1038/nclimate3206.

Melia, N., Dean, S., Pearce, H., Harrington, L., Frame, D., Strand, T., 2022. Aotearoa New Zealand's 21st-century wildfire climate. Earths Future 10 (6), e2022EF002853.

MfE, 2008. Climate change effects and impacts assessment: a guidance manual for local government in New Zealand. In: Mullan, B., Wratt, D., Dean, S., Hollis, M., Allan, S., Williams, T., Kenny, G. (Eds.), Prepared for Ministry for the Environment by, second ed. MfE, Wellington. NZ.

MfE, 2018. Climate change projections for New Zealand: atmospheric projections based on simulations from the IPCC fifth assessment. In: B, Sood, A., Stuart, S., Carey-Smith, T. (Eds.), Prepared for Ministry for the Environment by Mullan, second ed. Wellington, NZ.

Narsey, S., Brown, J.R., Delage, F., Boschat, G., Grose, M., Colman, R., Power, S., 2022. Storylines of South Pacific convergence zone changes in a warmer world. J. Clim. 35 (20), 2949–2967. https://doi.org/10.1175/JCLI-D-21-0433.1.

Neelin, J.D., Langenbrunner, B., Meyerson, J.E., Hall, A., Berg, N., 2013. California winter precipitation change under global warming in the Coupled Model Intercomparison Project phase 5 ensemble. J. Clim. 26 (17), 6238–6256.
Paeth, H., Hall, N.M., Gaertner, M.A., Alonso, M.D., Moumouni, S., Polcher, J., Ruti, P. M., Fink, A.H., Gosset, M., Lebel, T., 2011. Progress in regional downscaling of West African precipitation. Atmos. Sci. Lett. 12 (1), 75–82.
Palmer, T.N., Räisänen, J., 2002. Quantifying the risk of extreme seasonal precipitation events in a changing climate. Nature 415 (6871), 512–514.
Palmer, T., Stevens, B., 2019. The scientific challenge of understanding and estimating climate change. Proc. Natl. Acad. Sci. 116 (49), 24390–24395.
Pastor-Paz, J., Noy, I., Sin, I., Sood, A., Fleming-Munoz, D., Owen, S., 2020. Projecting the effect of climate change on residential property damages caused by extreme weather events. J. Environ. Manag. 276, 111012. https://doi.org/10.1016/j.jenvman.2020.111012.
Payne, A.E., Demory, M.-E., Leung, L.R., Ramos, A.M., Shields, C.A., Rutz, J.J., Siler, N., Villarini, G., Hall, A., Ralph, F.M., 2020. Responses and impacts of atmospheric rivers to climate change. Nat. Rev. Earth Environ. 1 (3), 143–157.
Pepin, N., Bradley, R.S., Diaz, H.F., Baraer, M., Caceres, E.B., Forsythe, N., Fowler, H., Greenwood, G., Hashmi, M.Z., Liu, X.D., Miller, J.R., Ning, L., Ohmura, A., Palazzi, E., Rangwala, I., Schöner, W., Severskiy, I., Shahgedanova, M., Wang, M.B., Mountain Research Initiative, E.D.W.W.G., 2015. Elevation-dependent warming in mountain regions of the world. Nat. Clim. Change 5 (5), 424–430. https://doi.org/10.1038/nclimate2563.
Perkins, S.E., Alexander, L.V., 2013. On the measurement of heat waves. J. Clim. 26 (13), 4500–4517.
Perkins-Kirkpatrick, S.E., Gibson, P.B., 2017. Changes in regional heatwave characteristics as a function of increasing global temperature. Sci. Rep. 7 (1), 12256. https://doi.org/10.1038/s41598-017-12520-2.
Pfahl, S., O'Gorman, P.A., Fischer, E.M., 2017. Understanding the regional pattern of projected future changes in extreme precipitation. Nat. Clim. Change 7 (6), 423–427. https://doi.org/10.1038/nclimate3287.
Pirooz, A., Moore, S., Carey-Smith, T., Turner, R., Su, C.-H., 2023. The New Zealand reanalysis (NZRA). Weather Clim. 42 (1), 58–74.
Prince, H.D., Cullen, N.J., Gibson, P.B., Conway, J., Kingston, D.G., 2021. A climatology of atmospheric rivers in New Zealand. J. Clim. 34 (11), 4383–4402.
Rampal, N., Gibson, P.B., Sood, A., Stuart, S., Fauchereau, N.C., Brandolino, C., Noll, B., Meyers, T., 2022. High-resolution downscaling with interpretable deep learning: rainfall extremes over New Zealand. Weather Clim. Extrem. 38, 100525.
Rampal, N., Hobeichi, S., Gibson, P.B., Baño-Medina, J., Abramowitz, G., Beucler, T., González-Abad, J., Chapman, W., Harder, P., Gutiérrez, J.M., 2024. Enhancing regional climate downscaling through advances in machine learning. Artif. Intell. Earth Sys. 3 (2), 230066. https://doi.org/10.1175/AIES-D-23-0066.1.
Rampal, N., Gibson, P.B., Sherwood, S., Abramowitz, G., Hobeichi, S., 2025. A reliable generative adversarial network approach for climate downscaling and weather generation. J. Adv. Model. Earth Syst. 17 (1), e2024MS004668. https://doi.org/10.1029/2024MS004668.
Renwick, J.A., Katzfey, J.J., Nguyen, K.C., McGregor, J.L., 1998. Regional model simulations of New Zealand climate. J. Geophys. Res. Atmos. 103 (D6), 5973–5982.
Rhoades, A.M., Jones, A.D., Srivastava, A., Huang, H., O'Brien, T.A., Patricola, C.M., Ullrich, P.A., Wehner, M., Zhou, Y., 2020. The shifting scales of western US landfalling atmospheric rivers under climate change. Geophys. Res. Lett. 47 (17), e2020GL089096.
Seneviratne, S.I., Donat, M.G., Pitman, A.J., Knutti, R., Wilby, R.L., 2016. Allowable CO2 emissions based on regional and impact-related climate targets. Nature 529 (7587), 477–483.
Sheffield, J., Wood, E.F., 2012. Drought: Past Problems and Future Scenarios. Routledge.
Shepherd, T.G., Boyd, E., Calel, R.A., Chapman, S.C., Dessai, S., Dima-West, I.M., Fowler, H.J., James, R., Maraun, D., Martius, O., Senior, C.A., Sobel, A.H., Stainforth, D.A., Tett, S.F.B., Trenberth, K.E., van den Hurk, B.J.J.M., Watkins, N.W., Wilby, R.L., Zenghelis, D.A., 2018. Storylines: an alternative approach to representing uncertainty in physical aspects of climate change. Clim. Change 151 (3), 555–571. https://doi.org/10.1007/s10584-018-2317-9.
Shu, J., Shamseldin, A.Y., Weller, E., 2021. The impact of atmospheric rivers on rainfall in New Zealand. Sci. Rep. 11 (1), 5869.
Sørland, S.L., Schär, C., Lüthi, D., Kjellström, E., 2018. Bias patterns and climate change signals in GCM-RCM model chains. Environ. Res. Lett. 13 (7), 074017.
Stone, D.A., Rosier, S.M., Bird, L., Harrington, L.J., Rana, S., Stuart, S., Dean, S.M., 2022. The effect of experiment conditioning on estimates of human influence on extreme weather. Weather Clim. Extrem. 36, 100427.
Swann, A.L.S., Hoffman, F.M., Koven, C.D., Randerson, J.T., 2016. Plant responses to increasing CO_2 reduce estimates of climate impacts on drought severity. Proc. Natl. Acad. Sci. 113 (36), 10019–10024. https://doi.org/10.1073/pnas.1604581113.
Thatcher, M., McGregor, J.L., 2009. Using a scale-selective filter for dynamical downscaling with the conformal cubic atmospheric model. Mon. Weather Rev. 137 (6), 1742–1752. https://doi.org/10.1175/2008MWR2599.1.
Trancoso, R., Syktus, J., Toombs, N., Ahrens, D., Wong, K.K.-H., Dalla Pozza, R., 2020. Heatwaves intensification in Australia: a consistent trajectory across past, present and future. Sci. Total Environ. 742, 140521.
Trenberth, K.E., 2011. Changes in precipitation with climate change. Clim. Res. 47 (1–2), 123–138.
Ukkola, A.M., De Kauwe, M.G., Roderick, M.L., Abramowitz, G., Pitman, A.J., 2020. Robust future changes in meteorological drought in CMIP6 projections despite uncertainty in precipitation. Geophys. Res. Lett. 47 (11), e2020GL087820. https://doi.org/10.1029/2020GL087820.
Vautard, R., Cattiaux, J., Happé, T., Singh, J., Bonnet, R., Cassou, C., Coumou, D., D'Andrea, F., Faranda, D., Fischer, E., Ribes, A., Sippel, S., Yiou, P., 2023. Heat extremes in Western Europe increasing faster than simulated due to atmospheric circulation trends. Nat. Commun. 14 (1), 6803. https://doi.org/10.1038/s41467-023-42143-3.
Vogel, M.M., Orth, R., Cheruy, F., Hagemann, S., Lorenz, R., van den Hurk, B.J.J.M., Seneviratne, S.I., 2017. Regional amplification of projected changes in extreme temperatures strongly controlled by soil moisture-temperature feedbacks. Geophys. Res. Lett. 44 (3), 1511–1519. https://doi.org/10.1002/2016GL071235.
Walters, D., Baran, A.J., Boutle, I., Brooks, M., Earnshaw, P., Edwards, J., Furtado, K., Hill, P., Lock, A., Manners, J., Morcrette, C., Mulcahy, J., Sanchez, C., Smith, C., Stratton, R., Tennant, W., Tomassini, L., Van Weverberg, K., Vosper, S., Willett, M., Browse, J., Bushell, A., Carslaw, K., Dalvi, M., Essery, R., Gedney, N., Hardiman, S., Johnson, B., Johnson, C., Jones, A., Jones, C., Mann, G., Milton, S., Rumbold, H., Sellar, A., Ujiie, M., Whitall, M., Williams, K., Zerroukat, M., 2019. The Met Office unified model global atmosphere 7.0/7.1 and JULES global land 7.0 configurations. Geosci. Model Dev. 12 (5), 1909–1963. https://doi.org/10.5194/gmd-12-1909-2019.
Williams, J., Morgenstern, O., Varma, V., Behrens, E., Hayek, W., Oliver, H., Dean, S., Mullan, B., Frame, D., 2016. Development of the New Zealand Earth system model. Weather Clim. 36, 25–44.
Yang, Y., Roderick, M.L., Zhang, S., McVicar, T.R., Donohue, R.J., 2019. Hydrologic implications of vegetation response to elevated CO2 in climate projections. Nat. Clim. Change 9 (1), 44–48. https://doi.org/10.1038/s41558-018-0361-0.
Zhang, X., Alexander, L., Hegerl, G.C., Jones, P., Tank, A.K., Peterson, T.C., Trewin, B., Zwiers, F.W., 2011. Indices for monitoring changes in extremes based on daily temperature and precipitation data. Wiley Interdiscip. Rev.: Clim. Change 2 (6), 851–870.